Probabilistic seismic performance assessment of an existing RC bridge with portal-frame piers designed for gravity loads only

Raffaele De Risi [a,*], Luigi Di Sarno [b], Fabrizio Paolacci [c]

[a] Department of Civil Engineering, University of Bristol, Queen's Building, University Walk, BS8 1TR Bristol, UK
[b] Department of Engineering, University of Sannio, Piazza Roma 21, 82100 Benevento, Italy
[c] Department of Engineering, Roma Tre University, Via Vito Volterra 62, 00146 Roma, Italy

ARTICLE INFO

ABSTRACT

The present analytical work illustrates a thorough assessment of the seismic performance of an existing reinforced concrete (RC) bridge with framed piers designed for gravity loads only. The seismic response is investigated through advanced, comprehensive and efficient dynamic non-linear analyses. The evaluation of the seismic performance for ductile and fragile components has been carried out with simplified yet reliable formulations, either based on codes or experimentally derived, partially validated with numerical simulations. The effects of far-field and near-source strong motions on the seismic response of the sample bridge have been assessed and discussed in details. Fragility curves are derived using both Cloud analysis and Incremental Dynamic Analysis (IDA) and considering two limit states, i.e. damage limitation and collapse. The outcomes of the refined numerical simulations show that the near-source strong motions tend to impose higher inelastic demand on fragile components of the bridge system than far-field records, nevertheless fragility curves relative to the latter records exhibit higher probability of failure than the near-source strong motion counterparts. For the damage assessment, it is found that the Cloud analysis lead to fragility curves similar to those derived through the IDA procedure. Finally, a new approach facilitating the preliminary identification of the weakest link of the bridge, namely the pier-by-pier fragility, is presented.

© 2017 Elsevier Ltd. All rights reserved.

1. Introduction

Widespread damage, partial and global collapses of bridges have frequently been surveyed in the aftermath of moderate-to-high magnitude earthquakes worldwide [9,26,13,65,41,40,64,74,72]. Most of the existing highway bridges, especially reinforced concrete (RC) bridges, were built without seismic details during the 60's and 70's; hence, their structural performance tends to be inadequate under earthquake ground motions [59,68,43,14,52,38,15]. Brittle failure due to limited shear capacity is a common damage pattern experienced by non-ductile reinforced concrete (RC) bridges (e.g. Fig. 1), especially those having portal-frame piers with short elements.

Structural failures can also be caused by the inappropriate connection between piers and footing, for an insufficient anchorage or lap splicing. Such damage pattern is exacerbated for RC bridge structures with smooth steel reinforcement, which is commonly found in existing RC bridges, especially those that were designed for gravity loads only as also proved during pseudo-dynamic [1] and dynamic shake table experimental tests [23]. The present analytical work assesses the earthquake performance of an existing RC bridge with portal-frame piers designed for gravity loads only, which is typically found in seismic-prone regions in the South of Europe. Novel research is focusing on existing sub-standard European bridges [51]; nonetheless, to Authors' knowledge, the present work is an early attempt to assess the Italian bridges with portal-frame piers designed for gravity loads.

The novelty of this work is the investigation of adequate formulations for the evaluation of the structural capacity of the elements of the piers according to existing structural codes and assessment guidelines [12,30,29,63]. Ductile and fragile components are assessed at two limit states: the significant damage limit state (DLS) and the collapse limit state (CLS). Moreover, a new simplified definition of the damageability to account also for the shear strength, based on the modified compression field theory, is proposed. Towards this aim, an existing RC Italian bridge located in the Emilia-Romagna region has been selected as case study.

* Corresponding author.
E-mail addresses: raffaele.derisi@bristol.ac.uk (R. De Risi), ldisarno@unisannio.it (L. Di Sarno), fabrizio.paolacci@uniroma3.it (F. Paolacci).

(a)　　　　　　　　　　　(b)

Fig. 1. Typical damage experienced by existing reinforced concrete bridges after an earthquake: detail of shear failure at the pier base, (a) Juan Pablo II Bridge affected by 2010 Chile Earthquake [72], (b) Moorhouse Avenue Overbridge affected by 2011 Christchurch earthquake [74].

The seismic response of the sample bridge has been investigated through advanced dynamic nonlinear analyses. To evaluate the record-to-record variability, according to the Pacific Earthquake Engineering Research (PEER) approach [16,50], two advanced structural analysis methods, i.e. the Cloud analysis [44,34,42,25,37] and the Incremental Dynamic Analysis (IDA) [69,70], have been employed. Both procedures are based on the selection of a suite of ground motions that are applied as they are in the case of Cloud analysis and are repeatedly scaled in the case of IDA. Performing both Cloud analysis and IDA facilitates the comparison of the two procedures, allowing also the identification of pros and cons of both methods. IDA is time consuming but it is suitable for a comprehensive structural assessment since it allows the evaluation of the relationship between engineering demand parameters (EDP) and intensity measures (IM) considering a large range of IM. On the other hand, it is nowadays common practice using automatic routines that perform structural analyses to prioritize the inspections on critical elements of the communication infrastructures, thus facilitating the emergency management [46]. Within such framework, Cloud analysis is very efficient since uses un-scaled ground motions, and requires relatively low computational efforts.

For the performed analyses, the seismic input is selected according to the disaggregation of the seismic hazard for the bridge location, using the results produced by Italian National Institute of Geophysics and Volcanology (INGV). The effects of far-field and near-source records have been assessed using two sets of thirty natural strong motions, in order to address the influence of these two types of ground motions on the structure [10]. An additional set containing both previously defined sets has also been investigated. To facilitate the understanding of the fragility curve for the bridge system as a whole, a new pier-by-pier fragility representation is proposed, in order to identify the "weakest link" in the systemic analysis of the bridge response.

The outcomes of the numerical simulations presented herein are part of a major research project funded by the European Community, i.e. "Assessment of the seismic vulnerability of an old RC viaduct with frame piers and study of the effectiveness of different isolation systems through pseudo-dynamic test on a large scale model (RETRO)". The RETRO project focuses on the experimental assessment of existing RC bridges structures [1,56,57,58].

2. Objective and methodology

In recent years, a great deal of research has focused on the definition of limit states and seismic assessment procedures for the existing structures, considering both structural and non-structural elements. Many efforts have been concentrated on residential buildings; for such structures a standard framework appears nowadays consolidated. Conversely, a common framework has not been established for the assessment of existing bridges. In the United States, numerous studies have focused on the observational results for bridges in the aftermath of historical earthquakes [49,75,4,27]. In Europe, especially in earthquake prone areas, such as Greece, Italy, and Turkey, significant research activities have also been carried out [31,10,38], but numerous definitions of limit states have emerged.

The present work aims at defining a general procedure for the seismic assessment of RC bridges designed primarily for gravity loads. It is recognized that future efforts should focus on the definition of the operational limit state to ensure the system functionality; notwithstanding the latter observation, this work accounts for the structural elements only, hence it does not account for the behavior of binder, road surface, pavement expansion joints, etc. It is, thus, a first attempt in the definition of a unified and reliable performance based assessment approach for existing RC sub-standard bridges. The proposed procedure comprises the following steps (see also Fig. 2): a) characterization of the structural system, b) limit states definition and selection of appropriate capacity formulations, c) seismic records selection, d) use of Cloud and/or IDA procedures, e) assessment of the seismic performance analyzing the results obtained from structural analyses, and, finally, f) selection of retrofitting scheme, if necessary.

The structural characterization comprises the collection of technical reports, drawings and tests data on materials. The above information allow the structural modeling of the bridge. Once the Performance Based Objectives (PBOs) have been characterized, appropriate limit states should be defined. Generally, the definition of the limit states is combined with appropriate capacity formulations for the structural elements. In this respect, appropriate capacity formulations are proposed herein; the selected capacity relationships are based on existing experimental and numerical studies hence they can be considered validated and accurate.
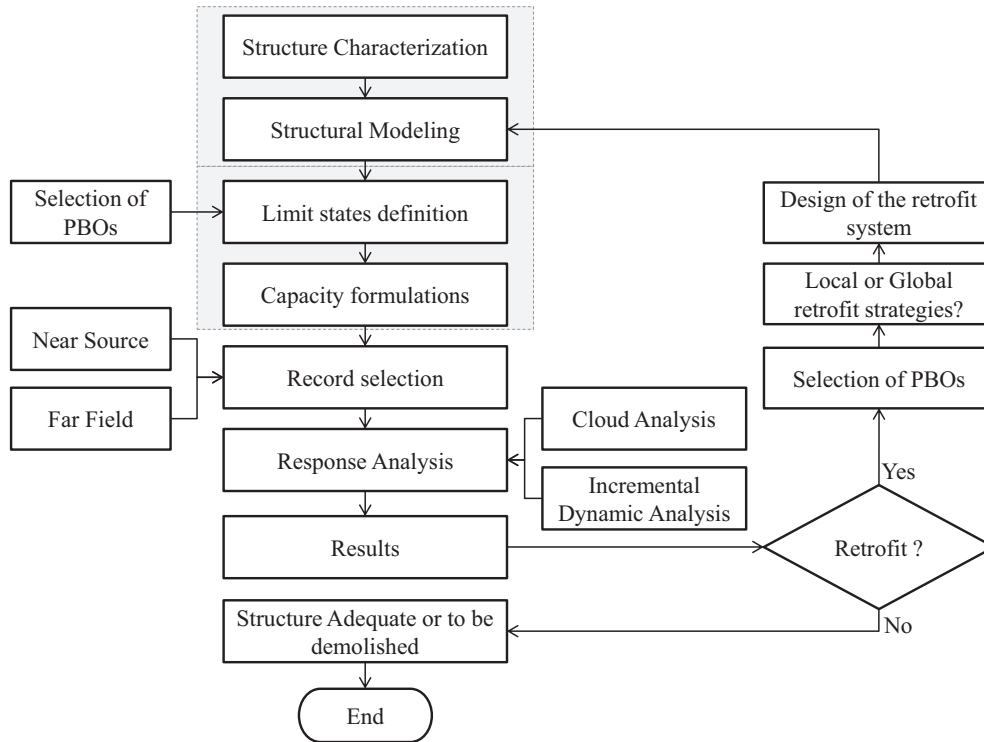
Fig. 2. The framework of structural performance assessment. (PBOs = Performance-Based Objectives).

The seismic assessment is then carried out through advanced non-linear dynamic analyses. It is thus essential to characterize accurately the seismic input. Using the seismic hazard disaggregation, near-source and/or far-field accelerograms can be selected, based on a given range of magnitude and epicentral distance values. Cloud and IDA procedures are used for the vulnerability analyses. The fragility curves can be used to either calculate the seismic risk, with the convolution of seismic hazard, or to calculate simplified risk indicator through the Demand Capacity Factored Design (DCFD) procedure [17]. Based on the level of acceptable risk, or simply on the acceptability of the demand-over-capacity ratio, it is possible to detect whether or not the seismic retrofitting is needed. If the bridge is structurally deficient, then the retrofitting scheme should be designed, and its effectiveness should be checked through the same procedure proposed for the assessment.

3. Sample bridge structure

The bridge used as sample structure is an existing reinforced concrete (RC) viaduct built in the 1970s; it is located in North-East of Italy, in the region of the 2012 Emilia Romagna (M_W = 5.9) earthquake [35]. The viaduct consists of a thirteen-span bay deck with two independent roadways resting on pairs of 12 portal frame piers, as displayed in Fig. 3. The portal frames comprise solid or hollow circular columns with diameters varying between 1.20 m and 1.60 m, connected at the top by a cap-beam and at various heights by one or more transverse beams of rectangular sections. The total length is equal to 421.10 m. The shortest span is 29.05 m long and the longest is 33.00 m. The minimum and maximum pier heights are 13.80 m (P12) and 41.34 m (P7), respectively. Fig. 3 provides the bridge longitudinal perspective and the structural system layout.

There are six intermediate Gerber saddles, acting as expansion joints; their location is indicated with circles in Fig. 3. For the sake

of simplicity, such saddles have been not accounted for in the present numerical studies and are modeled as pinned connections. The Gerber saddles influence the displacement profile of the deck. The first (T_1 = 1.61 s) and third (T_3 = 1.47 s) modes of vibration affect the left side of the deck (pile 1–6), meanwhile the second (T_2 = 1.55 s) ad fourth (T_4 = 0.89 s) modes affect the right side (pier 7–12).

Transverse RC diaphragms exist at the supports and also at intermediate locations in the span. There are also three intermediate diaphragms which are located in the first and last span, close to the abutments. The remaining spans of the bridge include 4 intermediate diaphragms. The deck has an open cross-section in the middle-span, as shown pictorially in Fig. 4. Due to the typical cross-sections of the bridge lanes (Fig. 4b), additional overturning moments may be experienced by the piers when subjected to horizontal seismic forces.

The top slab width and thickness are 10.75 m and 0.20 m, respectively; the two girder webs are 0.35 m thick; the total depth is 2.75 m. The cross-section of deck is a box girder close to the supports due to the addition of a bottom RC slab. Such additional slab has been neglected in the present analytical study. The bridge was designed with two decks for each road lane. Therefore, the system comprises two independent viaducts for both gravity and horizontal loads.

As shown in Fig. 5, the bridge piers have two types of column cross-sections: a solid circular section with diameter of 1200 mm and a hollow section with external and internal diameters equal to 1600 mm and 1000 mm respectively. The solid section has φ 20 mm bars whereas the hollow section includes φ 20 and φ 16 mm steel bars, for the external and internal reinforcement, respectively. The transversal reinforcement comprises a φ 6 mm steel spiral with a spacing of 140 mm. The transverse beams have a rectangular section with a width of 400 mm and height variable between 1200 mm and 1500 mm. The longitudinal reinforcements include φ 24 and φ20 steel bars. The transversal reinforcement
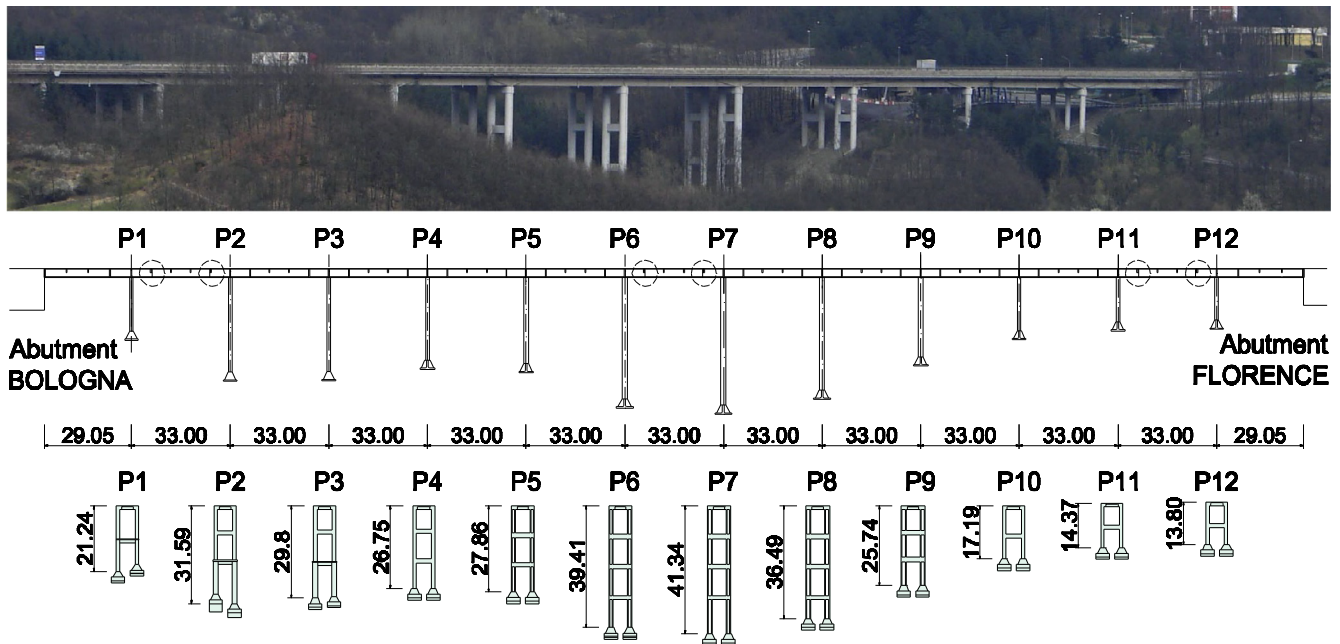
Fig. 3. The layout of the sample bridge.
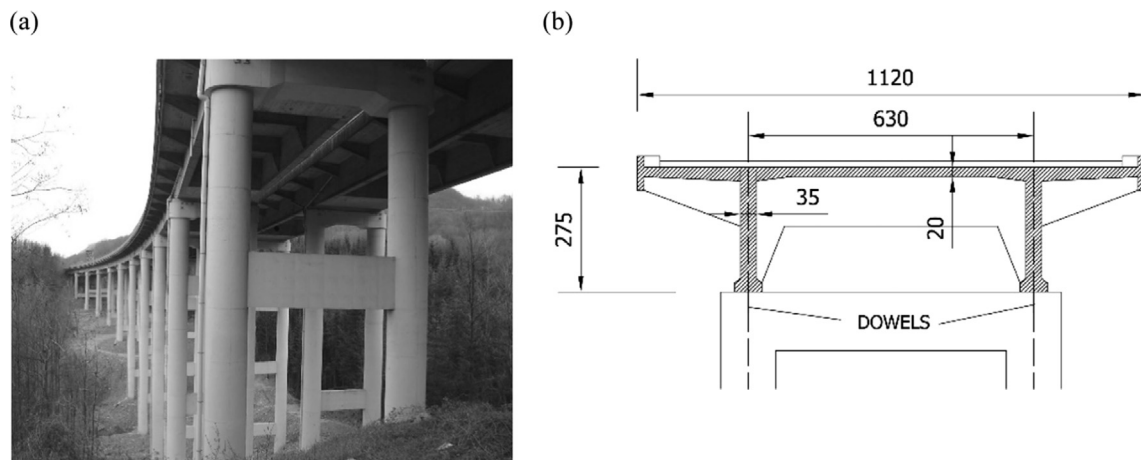
Fig. 4. Perspective view of the Rio Torto bridge (a) and transverse cross-section of the deck (b).

comprises φ8 steel bars with spacing of 200 mm and 45° inclined bars. The cap-beam of all the piers presents a U-shaped section. For such a beam, φ 18 longitudinal steel bars are used, whereas the transversal reinforcement includes φ 8 mm steel bars. Table 1 facilitates the identification of the piers and the relative levels of the cross-sections as per Fig. 5.

Each pier has a vertical load ranging between 4900 kN and 5600 kN (i.e. normalized axial load ν between 5% and 10%), being the length of the bays between 29 and 33 m. The structural steel, consisting of smooth reinforcement bars, has a mean yield strength of 350 MPa; the mean compressive resistance of the concrete is 26 MPa.

Experimental tests on scaled pier models [56,55] showed that shear failure may occur in the transverse beams of the framed pier, as displayed in Fig. 6a, as well as large crack openings may appear at column-foundation joint (Fig. 6b).

Finally, in this study, the sample bridge is assumed to be ideally straight, with a uniform cross section for the deck.

3.1. Structural modeling

A refined finite-element numerical model is implemented in OpenSees [47]. The following simplifications are considered: (1) the deck is represented as an elastic beam; (2) piers are fixed at the base and the fix-end rotation is modeled according to Zhao and Sritharan [77]; (3) flexibility of abutments was considered negligible, as further explained at the end of Section 4.1.3, and (4) interaction between the axial capacity and the shear strength is not modeled. However, piers are modeled by means of nonlinear fiber beam-column elements using a corrotational formulation, and the shear response is assumed elastic. No tension strength is considered for the concrete material; the compression behavior was simulated by the Mander model [45]. A bilinear model with 1% kinematic strain-hardening was used for steel rebars. A rigid transverse displacement restraint was assumed at the deck-to-abutment connections, whereas a free sliding option was selected for longitudinal displacements. Rigid vertical supports were

SECTION 1
16 Φ20 rebars
1200
stirrups Φ6 / 140

SECTION 2
20 Φ20 rebars
1600
stirrups Φ6 / 140

SECTION 3
out: 24 Φ20 rebars
1600
in: 14 Φ16 rebars
300
stirrups Φ6 / 150

SECTION 4
out: 20 Φ20 rebars
1600
in: 14 Φ16 rebars
300
stirrups Φ6 / 150

SECTION 5
top: 4 Φ24 + 8 Φ20
1400
350
1400
wall: 4 Φ8
st. Φ8/200
400
bottom: 4 Φ24 + 8 Φ20

SECTION 6
1200
top: 16 Φ18
wall: 17 Φ8
st. Φ8/200
1200
bottom: 16 Φ18

SECTION 7
1200
top: 8 Φ18
200
wall: 17 Φ8
st. Φ8/200
1000
1200
300 | 600 | 300
bottom: 8 Φ18

SECTION 8
1200
top: 4 Φ18
200
wall: 17 Φ8
st. Φ8/200
1000
1200
300 | 600 | 300
bottom: 4 Φ18

SECTION 9
top: 4 Φ24 + 8 Φ20
wall: 4 Φ8
st. Φ8/200
1300
400
bottom: 4 Φ24 + 8 Φ20

SECTION 10
top: 4 Φ24 + 6 Φ20
wall: 4 Φ8
st. Φ8/200
1300
400
bottom: 4 Φ24 + 6 Φ20

SECTION 11
top: 4 Φ24
wall: 4 Φ8
st. Φ8/200
1300
400
bottom: 4 Φ24

SECTION 12
top: 4 Φ24 + 4 Φ20 + 4 Φ18
wall: 4 Φ8
st. Φ8/200
1500
400
bottom: 4 Φ24 + 4 Φ20 + 4 Φ18

SECTION 13
top: 4 Φ24 + 8 Φ20
wall: 4 Φ8
st. Φ8/200
1500
400
bottom: 4 Φ24 + 8 Φ20

SECTION 14
top: 4 Φ24
wall: 4 Φ8
st. Φ8/200
1500
400
bottom: 4 Φ24

SECTION 15
top: 4 Φ24 + 8 Φ20
wall: 4 Φ8
st. Φ8/200
1200
400
bottom: 4 Φ24 + 8 Φ20

SECTION 16
top: 4 Φ24
wall: 4 Φ8
st. Φ8/200
1200
400
bottom: 4 Φ24

Fig. 5. Pier cross-sections (units: mm).

Table 1
Key table relating section IDs to piers and levels.

Levels		Sections															
		1	2	3	4	5	6	7	8	9	10	11	12	13	14	15	16
Piers	1	1;2				1	2	2	2								
	2	2;3	1			1	3	3	3	2	2	2					
	3	2;3	1			1	3	3	3	2	2	2					
	4	1;2;3					3	3	3	2;3	2;3	2;3					
	5			1;2	3		3	3	3	1	1	1	2	2	2		
	6			1;2	3;4		4	4	4	1	1	1	2;3	2;3	2;3		
	7			1;2	3;4		4	4	4	1	1	1	2;3	2;3	2;3		
	8			1;2	3;4		4	4	4	1	1	1	2;3	2;3	2;3		
	9			1;2	3		3	3	3								
	10	1;2					2	2	2							1	1
	11	1;2					2	2	2							1	1
	12	1;2					2	2	2	1	1	1					

Fig. 6. Typical shear and flexural damage occurred respectively in the transverse beams and column of the experimental scaled model (after [55]).

assumed at the bearing locations. Additional details on modeling issues for this bridge can be found in Paolacci et al. [58] and Abbiati et al. [1].

4. Seismic fragility assessment

The fragility assessment is carried out with the Cloud and Incremental Dynamic Analysis (IDA) procedures. The peak ground acceleration (PGA) is adopted as intensity measure (IM); PGA was identified by Nielson and DesRoches [53] and Padgett et al. [54] as a reliable measure, for sufficiency and efficiency, for the seismic structural assessment of bridges. Similar results are obtained by Zelaschi et al. [76]. It is worth mentioning that further studies are needed to investigate whether or not the PGA is an all-embedded, efficient and sufficient IM to be used in studies similar to the present analytical investigation. It is authors' opinion that PGA is a simple but robust IM that can be reliably utilized for the comparisons discussed in the next sections.

The engineering demand parameter (EDP) is the critical demand-to-capacity ratio (Y_{LS}) and is defined as the demand-to-capacity ratio for the structural components that brings the structural system to exceed a given limit state. According to the basic principles of the Load and Resistance Factor Design (LRFD), the onset of a given limit state is not considered as a progressive damage/collapse analysis of the structure, but it is defined as the first local failure, i.e. the first attainment of the chord rotation capacity or the reaching of the shear strength.

The adopted framework is based on the cut-set concept [24], which is suitable for cases where various potential failure mechanisms affect the structural response, and it is even more common for bridge assessment [8,32]:

$$Y_{LS} = \max_{l}^{N_{mech}} \min_{j}^{N_l} \frac{D_{jl}}{C_{jl}(LS)} \tag{1}$$

where N_{mech} is the number of considered potential failure mechanisms and N_l the number of components taking part in the lth mechanism. D_{jl} and $C_{jl}(LS)$ are respectively the demand and the capacity of the jth component of the lth mechanism. As far as the system reliability is concerned, a cut-set is defined as any set of components whose joint failure implies failure of the system (i.e. $Y_{LS} > 1$).

In this work, three different sets of EDP have been considered, namely the pure flexural critical demand-to-capacity ratio $Y_{LS,f}$ (i.e. only the failure mechanisms related to the chord rotation in the elements are considered), the mechanism critical demand-to-capacity ratio (i.e. all the potential soft-storey or global mechanism are pre-identified and monitored during the analyses), and the overall demand to capacity ratio Y_{LS} that takes into account also the brittle failure in the structural elements, especially in the transversal beams. The above EDPs can be considered sufficient and adequate to reliable characterize the seismic performance of the analyzed bridge.

4.1. Limit states and capacity formulations

Two limit states (LSs) were considered for the structural performance assessment of the sample bridge structure: severe damage limit state (DLS) and collapse (CLS) limit state. Such selection is compliant with typical code-based bridge seismic performance evaluation [12,30,63]. At the onset of CLS the closure to the traffic is expected for demolition and reconstruction, with consequent direct and indirect losses. The most vulnerable components of the sample bridge model are the portal-frame piers. The deck, the pier foundations and the abutments are not included in the present analysis. Specifically, it has been observed that for non-skewed bridges the principal structural elements are more important than the other aspects [39,48].

The piers tend to fail whether shear strength or chord-rotation limit is exceeded. According to the experimental activity performed in the laboratory of Roma Tre University [55], it was possible to identify the damage distribution at increasing level of lateral displacement, thus checking the consistency of the collapse limit states adopted in the following sub-sections.

4.1.1. Collapse limit state (CLS)

According to the definition of $Y_{LF,f}$ and Y_{LS} in Eq. (1), the flexural capacity and the shear capacity have been considered. Moreover, given the cross-section type of the pier columns, the strength is computed with different formulations for the transverse beams and the columns.

4.1.1.1. Ductile mechanisms.
The chord rotation capacity of columns and beams is computed as provided below [28]:

$$\theta_u = \theta_y + (\phi_u - \phi_y) \cdot L_{pl} \cdot \left(1 - 0.5 \cdot \frac{L_{pl}}{L_V}\right) \tag{2}$$

where θ_y is the chord rotation at yielding, ϕ_u and ϕ_y are the ultimate and yielding section curvatures respectively. The latter curvatures are computed with respect to the maximum concrete deformation (assumed equal to 0.5%, as suggested by Reluis Guideline, 2009). L_{pl} is the plastic hinge length assumed equal to the 10% of the element height, since the formulation below can be approximated to that value (i.e. the yield penetration has been neglected):

$$L_{pl} = 0.10 \cdot H + 0.015 \cdot f_y \cdot d_{bL} \tag{3}$$

where f_y is the yielding strength of the reinforcement bars and d_{bL} is the longitudinal bar diameter. Additionally, L_V is the shear length and it is assumed equal to half of the structural element length.

For the column at the pier base, the contribution due to the fixed-end rotation was also considered. The formulation proposed by Biskinis and Fardis [7]:

$$\theta_u = \theta_y + (\phi_u - \phi_y) \cdot L_{pl} \cdot \left(1 - 0.5 \cdot \frac{L_{pl}}{L_V}\right) + a_{sl} \cdot \Delta\theta_{u,slip} \tag{4}$$

where a_{sl} is equal to 1 and $\Delta\theta_{u,slip}$ is given by the equation:

$$\Delta\theta_{u,slip} = 5.5 \cdot d_{bL} \cdot \phi_u \tag{5}$$

Differently from Eq. (2), the term L_{pl} in Eq. (4) is now evaluated accordingly to the work by Biskinis and Fardis [7]; hence it follows:

$$L_{pl} = 0.6 \cdot H \cdot \left[1 + \frac{1}{6} \cdot \min\left(9, \frac{L_V}{D}\right)\right] \tag{6}$$

The above relationship for L_{pl} is different from the previous one presented in Eq. (3), but it is coherent with the formulation used for the structural check of the section at the base.

Eqs. (2) and (4) should be further modified to account for the presence of plain bars, as in the case of the sample bridge. Correction coefficients (i.e. multiplier of the theoretical formulations) based on experimental tests have been suggested in the literature. Fardis [28] proposed a coefficient k that depends on a ratio between lap splice length l_o and d_{bL}. For values of $l_o/d_{bL} > 40$, the coefficient k is equal to 0.75. This correction coefficient is similar to that proposed in CEN [12]. More recently, Verderame et al. [71] performed a further accurate calibration of this coefficient based on a large tests database, suggesting the adoption of the following correction function: $k = 0.02 \min(50, l_o/d_{bL})$. In the case study considered herein, the factor $l_o/d_{bL} > 50$, therefore $k = 1$ and no correction coefficient is necessary.

4.1.1.2. Fragile mechanisms. The shear strength of the circular sections and the beams is computed in compliance with the EC8 formulation [12]:

$$V_R = \frac{H-x}{2 \cdot L_V} \cdot \min(N, 0.55 \cdot A_c \cdot f_c) + [1 - 0.05 \cdot \min(5, \mu_{\Delta,pl})] \cdot$$
$$\cdot \left\{ 0.16 \cdot \max(0.5, 100 \cdot \rho_{tot}) \cdot \left[1 - 0.16 \cdot \min\left(5, \frac{L_V}{H}\right) \right] \cdot \sqrt{f_c} \cdot A_c \right\} + V_W \tag{7}$$

where x is the neutral axis depth at yielding, N is the axial load in the element, A_c is the section area, f_c is the cylindrical compression strength, ρ_{tot} is the total geometric percentage of longitudinal steel reinforcement, and $\mu_{\Delta,pl}$ is the ductility, conservatively set equal to 5. Finally, the term V_W is the shear strength due to the transversal reinforcement, which is given for the rectangular sections as follows:

$$V_W = \rho_w \cdot b \cdot z \cdot f_y \tag{8}$$

and for circular sections is as below:

$$V_W = \frac{\pi}{2} \cdot \frac{A_{sw}}{s} \cdot f_y \cdot (H - 2c) \tag{9}$$

where ρ_w is the geometrical percentage of transversal reinforcement for the rectangular section, b is the section base, z is the internal lever arm, A_{sw} is the area of the circular stirrups, s is the stirrups spacing, and c is the concrete cover.

For hollow circular sections, the formulation proposed by Ranzo and Priestley [61] and Priestley et al. [60] has been adopted:

$$V_R = V_c + V_s + V_p \tag{10}$$

where V_c, V_s and V_p account for the contribution provided by the concrete, shear reinforcement and axial load, respectively. Considering the shape of pier cross-sections, namely circular solid and hollow sections, the strength derived from the formulation presented above has been compared with the results obtained from computer-platform Response 2000 [6], a powerful and reliable computational tool based on the modified compression field theory. The comparison between results obtained by using Response 2000 and those derived from Eq. (10) is presented in Fig. 7.

In Fig. 7 the results for the solid circular sections are depicted with hollow circles, while the results for the hollow sections are indicated with the filled circles. The comparisons show that for both types of sections, the ratios between the strengths calculated with the two formulations are close to unity, the maximum
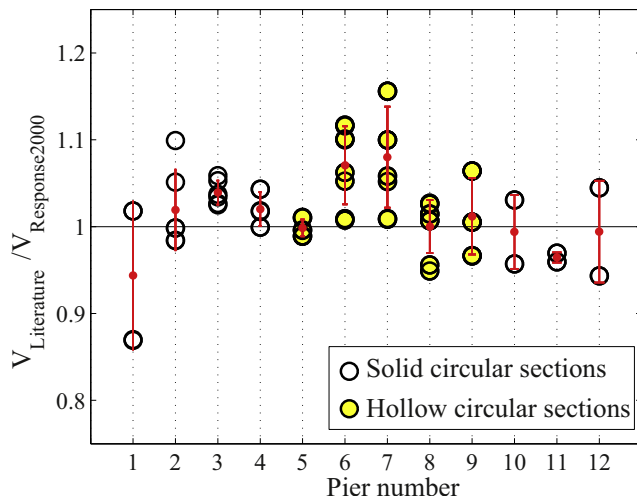
Fig. 7. Comparison between literature shear strength formulations and Response 2000 values.

variation is 12%. Additionally, for each pier, the mean ratio (the red solid dot) tends to the unity; the dispersion of the computed results is limited as shown by the red line in the diagram.

4.1.2. Significant damage limit state (DLS)
Both flexural and brittle mechanisms have been considered for the assessment of the response of columns and beams.

4.1.2.1. Ductile mechanisms. The yielding rotation for the columns is calculated as suggested by [28]:

$$\theta_y = \phi_y \cdot \frac{L_V}{3} \tag{11}$$

For the base column sections, the contribution of the fixed-end rotation is also considered according to Biskinis and Fardis [7]:

$$\theta_y = \phi_y \cdot \frac{L_V + a_V \cdot z}{3} + 0.0027 \cdot \left[1 - \min\left(1, \frac{2}{15} \cdot \frac{L_V}{H} \right) \right]$$
$$+ a_{sl} \cdot \frac{\phi_y \cdot d_{bL} \cdot f_y}{8 \cdot \sqrt{f_c}} \tag{12}$$

where a_V and a_{sl} are equal to unity for the present case study.

For the beam, the yielding chord rotation is evaluated according to [28]:

$$\theta_y = \phi_y \cdot \frac{L_V}{3} + 0.0013 \cdot \left(1 + 1.5 \cdot \frac{H}{L_V} \right) + 0.13 \cdot \frac{\phi_y \cdot d_{bL} \cdot f_y}{\sqrt{f_c}} \tag{13}$$

4.1.2.2. Fragile mechanisms. As far as the shear is concerned, in the present work, a shear threshold (i.e. a strength) has been suggested for the DLS. The evaluation of such threshold on a thorough study of the response of structural elements has been carried out with the modified compression field theory using computer-platform Response 2000 [6]. The ratio of the maximum shear and the shear corresponding to the elastic behaviour identified on the pushover curve for each element derived by means of Response 2000 is computed. Fig. 8 illustrates the pushover response curves for the columns and the beams, respectively, modeled as elements with length equal to the shear-length.

It is observed that the ratio between maximum shear and the shear corresponding to the elastic behaviour (represented by the filled circles in Fig. 8) is equal to about 2 for the columns and about 5 for the beams. These values have been used to scale-down the ultimate shear strengths, presented in Eqs. (7) and (10) to compute the shear limitation for the DLS. This is fully consistent with the experimental tests and numerical simulations performed at Roma Tre University [55], and with results presented in Del Vecchio et al. [22], where a rigorous analysis with Vector 3D has been performed on the same very piers of Rio Torto viaduct.

4.1.3. Further considerations
Structural elements of piers such as columns and beams are the focus of the structural analyses; on the other hand, additional relevant elements should be considered, such as the deck behaviour, foundations and their geotechnical aspects, connections between piers and deck, deck saddles, abutment supports, and abutment systems with the inherent geotechnical problems. Several hypotheses are made herein on the modeling of such elements because this work is an early attempt to analyze European bridge with portal-frame piers, therefore for such structures is more appropriate a gradual understanding; hence emphasis should be on structural piers.

As far as the deck is concerned, it exhibits an elastic response thus it does not impair the seismic response of the bridge. With respect to the geotechnical problems, since the piers foundations are massive footings without any indirect foundation elements
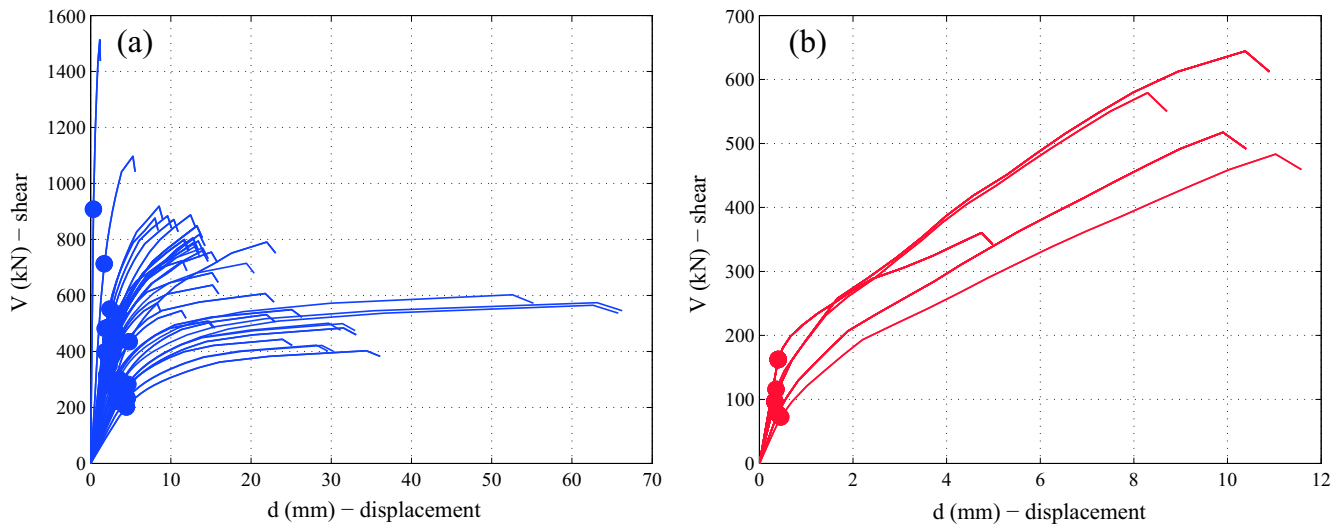
Fig. 8. Response 2000 results for columns (left) and beams (right).

(i.e., piles), and given the class B of the soil, it can be reliably assumed that the geotechnical response is less influencing than the structural behavior in a performance based framework for seismic assessment. Soil-structure interaction and abutment-soil interaction is beyond the scope of the present paper.

Regarding connections between piers and deck, the original design shows that for each pier there are 4 dowels having diameter 34 mm, and a steel tensile yielding strength of 350 MPa. Applying the formulation proposed by Vintzēleou and Tassios [73] the shear strengths of the connection associated to dowels is equal to about 400 kN. Given the direct contact between deck and piers, also the friction between the two concrete elements participate to the final strength. Assuming a friction coefficient of 0.3 [33] and considering a mean load transferred from the deck to each pier of 5600 kN, an extra-resistance of 1680 kN is added to the connection strength. Summing up the two contributions, the connection strength is much larger than the shear obtained from the seismic analysis, as observed in the next sections. Therefore, the influence of connection between piers and deck is neglected hereafter: the two concrete beams of the deck are considered simply hinged to the pier.

Regarding internal saddles and supports, such internal restraints are modeled as hinges. Therefore, the potential loss of support is not considered in the performed nonlinear analyses. The latter approach may appear as a limitation of present work; nevertheless, it is in line with the general purpose of this paper to investigate primarily the main structural elements of the bridge system.

Finally, potential incoherence problems were also not explicitly accounted for in the present assessment. However, it is worth emphasizing that the dynamic behavior of the bridge interests the two half of the bridge (long about 200 m) in an uncoupled manner, and a length of 400 m is identified as the limit over which the problem of coherence should be taken into account [66,67].

4.2. Record selection

In the present analytical study, only the record-to-record variability is considered. The record selection is based on the deaggregation results, freely available online at the INGV internet website (http://esse1-gis.mi.ingv.it/s1_en.php). Fig. 9(a) shows the bridge location with respect the Italian seismogenic zones and Fig. 9(b) shows the deaggregation results for that location.

Two sets of 30 natural earthquake records are selected in order to distinguish between the near-source (herein defined as records with epicentral distance less than 15 km, indicated as set A and listed in Table 2) and far-field (i.e. records with epicentral distance >15 km and less than 30 km, indicated as set B, listed in Table 3) records. The suite of strong motion records is collected from European Strong Motion Database [3]. The sample records are mainshock free-field records, including only the most severe (in terms of PGA) of the two horizontal components for the same registration. The soil property of the record stations is characterized as stiff soil (400 m/s < $Vs_{,30}$ < 700 m/s), in compliance with the Eurocode 8 [11] soil type B (i.e. the soil type for the site of the bridge case study). The set A records have moment magnitude (M_W) between 4.1 and 6.0 and epicentral distance (ED) between 1 km and 14 km. The set B possesses M_W ranging between 4.2 and 6.0 but ED between 16 km and 30 km. Tables 1 and 2 provide also the dominant period (T_P) [62], the mean period (T_m) [62] and the significant duration (D) [18] of the ensemble of records used for the non-linear response history analyses.

Although the direction of application of the seismic record is an important issue [20], the sample records of selected sets include a single strong motion for each event, considering a single direction only, since only the transversal bridge direction has been investigated herein, being the most vulnerable one [1].

It is thus possible to obtain independent records [25], i.e. record of different events. This is a crucial assumption for proceeding with the Cloud approach. The study is completed considering also a third set made of all the records belonging to the two sets together. This third set has been used primarily to make further considerations on the fragilities. Fig. 10 illustrates the elastic response spectra in terms of accelerations for the selected ground motion records. The response spectra are evaluated for 5%-equivalent viscous damping coefficients. The median spectrum (solid lines in Fig. 10) and the 16th and 84th percentile spectra (dotted lines) are also plotted in the same figure.

5. Preliminary response analysis

The response of the bridge is preliminarily assessed in terms of peak top pier lateral displacement, base shear and lateral drift. Since the sets of records include a number of accelerograms greater than seven, the effects on the structure are reported hereafter as the mean value of the maximum response parameter above defined, as suggested by the European seismic Standards [11].
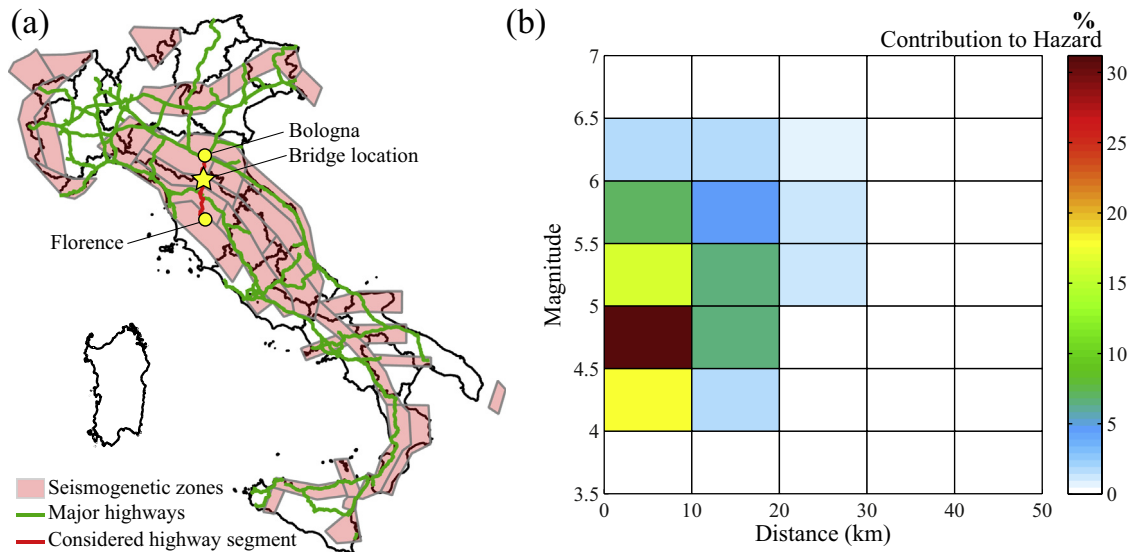
Fig. 9. (a) Bridge location with respect to the Italian highway networks and the seismogenetic zones; (b) Seismic deaggregation results.

Table 2
The set of 30 ground motions records belonging to set A (na = not available).

	Record	Date	M_W	Fault Mechanism	R [km]	PGA [g]	T_P [s]	T_m [s]	D [s]
1	Holt	26/08/1986	4.6	na	14	0.071	0.23	0.23	1.79
2	Dursunbey	18/07/1979	5.3	Normal	6	0.288	0.23	0.26	2.48
3	Near coast of Preveza	31/08/1985	5.2	Oblique	13	0.087	0.27	0.29	7.66
4	Kyllini	16/10/1988	5.9	Strike slip	14	0.151	0.53	0.43	15.67
5	Patras	22/12/1988	4.9	Normal	5	0.111	0.58	0.44	3.80
6	Umbria	03/09/1997	4.5	Normal	13	0.295	0.15	0.15	1.42
7	Ano Liosia	07/09/1999	6.0	Normal	14	0.326	0.17	0.27	5.61
8	Aghios Vasileios	18/02/1986	4.8	na	12	0.018	0.44	0.33	7.93
9	Mikrothivai	30/11/1987	4.4	na	14	0.032	0.47	0.36	10.20
10	Kefallinia island	24/08/1990	4.5	na	9	0.079	0.13	0.14	1.76
11	Ierissos	26/08/1983	5.1	Strike slip	8	0.183	0.23	0.30	3.28
12	Paliouri	10/04/1994	5.1	na	5	0.068	0.34	0.35	2.88
13	Patras	14/07/1993	5.6	Strike slip	9	0.340	0.40	0.24	6.05
14	Sarti	24/02/1993	4.4	na	7	0.115	0.09	0.12	0.72
15	Near SW coast of Levkas island	21/07/1990	4.3	na	4	0.046	0.33	0.26	6.25
16	Komilion	25/02/1994	5.4	Oblique	12	0.057	0.39	0.40	11.57
17	Ionian	27/02/1994	4.8	Thrust	14	0.035	0.34	0.26	9.95
18	Levkas island	18/07/1994	4.9	na	9	0.064	0.34	0.37	7.14
19	Near E coast of Zakynthos island	24/05/1990	4.8	na	2	0.035	0.29	0.26	9.53
20	Mazarron	02/09/1996	4.4	Oblique	1	0.006	0.19	0.36	12.09
21	Ventas de Huelma	24/02/1997	4.2	Oblique	10	0.045	0.17	0.20	7.70
22	Oelfus	13/11/1998	5.1	Oblique	11	0.147	0.62	0.30	1.80
23	Holt	23/04/1991	4.7	na	4	0.124	0.23	0.23	2.90
24	Araxos	06/03/1997	4.1	na	9	0.026	0.09	0.13	4.63
25	Gulf of Corinth	22/02/1997	4.2	Normal	13	0.039	0.22	0.19	5.05
26	Near coast of Katerini	07/04/1997	4.1	na	12	0.005	0.17	0.23	8.56
27	Off coast of Kefallinia island	26/05/1996	4.7	na	8	0.019	0.15	0.28	8.50
28	Zakynthos island	17/10/1994	4.6	na	3	0.024	0.10	0.19	8.03
29	Firuzabad	20/06/1994	5.9	Strike slip	7	1.065	0.20	0.18	5.57
30	Masjed-E-Soleyman	25/09/2002	5.6	Thrust	13	0.062	0.25	0.25	13.48
	Mean		4.9		9.2	0.13	0.28	0.27	6.47
	Standard deviation		0.6		4.0	0.20	0.14	0.09	3.87

Moreover, non-linear static (pushover) analyses have been performed to compute the ultimate top displacement (δ_{CLS}) and the corresponding base shear (V_{CLS}) for each pier. The latter structural response parameters are used hereafter to normalize the mean results in terms of displacements and base shear, respectively.

5.1. Peak top pier lateral displacement

The mean values of maximum transversal displacements of the deck and piers, for near- and far-field records, are shown in Fig. 11.

The results in the figure refer to the near-source and far-field set of accelerograms; they are displayed in red and blue, respectively.

For the near-source ground motions, the mean transversal deck displacements (and consequently the transversal top pier displacements) are slightly greater than the results obtained for the far-field ground motions. On the other hand, the 90% confidence interval is much larger, reflecting the higher variability of the spectral response shown in Fig. 10.

Fig. 12 shows the normalized transversal displacement for each pier for both sets of selected accelerograms. The normalization of

Table 3
The set of 30 ground motions records belonging to set B (na = not available).

	Record	Date	M_W	Fault Mechanism	R [km]	PGA [g]	T_P [s]	T_m [s]	D [s]
1	Basso Tirreno	15/04/1978	6.0	Oblique	18	0.152	0.23	0.28	8.00
2	Montenegro	09/04/1979	5.4	Thrust	18	0.071	0.40	0.37	7.73
3	Valnerina	19/09/1979	5.8	Normal	23	0.043	0.18	0.26	12.42
4	Preveza	10/03/1981	5.4	Thrust	28	0.143	0.37	0.34	9.19
5	Umbria	29/04/1984	5.6	Normal	19	0.209	0.12	0.17	5.12
6	Javakheti Highland	16/12/1990	5.4	Strike slip	29	0.118	0.32	0.28	4.97
7	Izmir	06/11/1992	6.0	Strike slip	30	0.039	1.40	0.98	11.85
8	Gulf of Corinth	04/11/1993	5.3	Normal	18	0.027	0.27	0.26	6.50
9	Komilion	25/02/1994	5.4	Oblique	29	0.035	0.94	0.66	14.27
10	S of Parma	09/11/1983	5.0	Oblique	18	0.033	0.33	0.35	6.58
11	Potenza	05/05/1990	5.8	Strike slip	28	0.096	0.36	0.35	11.15
12	Ano Liosia	07/09/1999	6.0	Normal	16	0.307	0.22	0.27	4.42
13	Epagny	15/07/1996	4.2	Strike slip	29	0.008	0.25	0.27	9.72
14	Harbiye	22/01/1997	5.7	Oblique	19	0.148	0.51	0.31	15.04
15	Samos	02/04/1996	5.4	Normal	26	0.033	0.31	0.21	6.32
16	Etolia	22/05/1988	5.4	Thrust	21	0.039	0.13	0.20	8.84
17	Kefallinia island	02/06/1988	4.8	na	18	0.016	0.21	0.33	10.83
18	Gulf of Corinth	05/07/1988	4.9	Normal	19	0.076	0.24	0.25	11.44
19	Near NE coast of Crete	09/02/1987	4.9	na	22	0.010	0.24	0.31	8.93
20	Near SE coast of Zakynthos island	04/10/1984	5.0	na	17	0.079	0.32	0.28	8.78
21	Kyllini	16/10/1988	5.9	Strike slip	16	0.029	0.19	0.20	6.83
22	Cresta di Reit	29/12/1999	4.9	Normal	30	0.023	0.14	0.16	4.56
23	Mt. Hengill Area	04/06/1998	5.4	Strike slip	21	0.038	0.57	0.46	6.81
24	Jesreel Plain	24/08/1984	5.3	Oblique	18	0.030	0.17	0.21	7.00
25	Itea	05/11/1997	5.6	Oblique	28	0.058	0.29	0.26	9.94
26	S of Vathi	05/11/1997	4.6	na	26	0.021	0.23	0.20	9.37
27	Zakynthos Island	16/02/1997	4.9	na	20	0.008	0.30	0.31	7.37
28	Rhodos island	26/04/1996	5.4	Oblique	19	0.012	0.15	0.20	7.32
29	Off coast of Levkas island	01/12/1994	5.3	Strike slip	19	0.082	0.39	0.35	8.30
30	Aigion	08/04/2001	4.2	Oblique	17	0.035	0.13	0.13	4.99
	Mean		5.30		21.97	0.07	0.33	0.31	8.49
	Standard deviation		0.48		4.86	0.07	0.26	0.16	2.76

the top pier lateral displacement (δ) is carried out with reference to the DLS and CLS capacity values (i.e. δ_{DLS} and δ_{CLS}) computed with the pushover analysis, as also suggested elsewhere [21]. The capacity values are defined as the top pier displacement at the onset of DLS and CLS evaluated according the capacity formulations described in Section 4.1.

It is worth noting that only peaks vary passing from absolute displacements (Fig. 11) to normalized displacements (Fig. 12); latter observation is due to the relative influence of demand and capacity.

Moreover, it is observed that the displacement corresponding to DLS is exceeded in several circumstances for both sets of accelerograms, whereas the displacements corresponding to the collapse is reached only for high percentiles of the response; such circumstance is found for near-source earthquake ground motions.

5.2. Base shear

Fig. 13 shows the mean of the maximum base shear values in the piers. Such base shear values have also been normalized with respect to the DLS and CLS capacity values (i.e. V_{DLS} and V_{CLS}); such normalization is shown in Fig. 14. The capacity values for each pier are defined as the pier base shear (evaluated with a pushover analysis) at the onset of DLS and CLS evaluated according the capacity formulations described in Section 4.1. The same trend described for the transversal displacements of the deck, can be observed.

5.3. Maximum demand-over-capacity ratio

The maximum demand-over-capacity ratio for each pier for the sample suites of earthquake records is herein analyzed. Results obtained by using the Eq. (1), are summarized in Fig. 15.

It is noted that the critical response concerns piers # 11 and #12, which are short piers characterized by shear response, thus

confirming the outcomes of recent experimental laboratory tests (see also Abbiati et al. [1] and Paolacci et al. [56]).

6. Fragility analysis

6.1. Cloud-based fragility curves

The Cloud Analysis implements non-linear dynamic analyses through (linear) regression-based probabilistic model [5]. This model can be expressed as follows:

$$E[\log Y|PGA] = \log \eta_{Y|PGA} = \log a + b \log PGA$$
$$\beta_{\log Y|PGA} = \sqrt{\frac{\sum_{i=1}^{n}(\log Y_i - \log \eta_{Y|PGA})^2}{n-2}} \tag{14}$$

where $\eta_{Y|PGA}$ is the median for Y given PGA and $\beta_{\log Y|PGA}$ is the logarithmic standard deviation for Y given PGA. Figs. 16 illustrates the results of the Cloud analysis considering the near-source (a, d), far-field (b, e) sets of records, and both sets together (c, f). The linear regression for the flexural critical demand to capacity ratio ($Y_{DLS,f}$ and $Y_{CLS,f}$, results in black) and the overall critical demand-to-capacity ratio (Y_{DLS} and Y_{CLS}, results in red, blue, and magenta) have also been included in the same figures. The dispersion around the median value tends to be large; notwithstanding, the significance of the regressions is satisfied.

Fig. 16 shows that the results relative to the brittle failure (the linear regressions shown in red, blue, and magenta) tend to reach the limit state (i.e. Y = 1) for spectral acceleration values smaller than for the case of the flexural case-only (the linear regressions presented in black). Moreover, dispersion values computed for the far-field records are larger with respect to the values obtained with the near-source strong motions. The robust fragility curve was built according to Jalayer et al. [36].
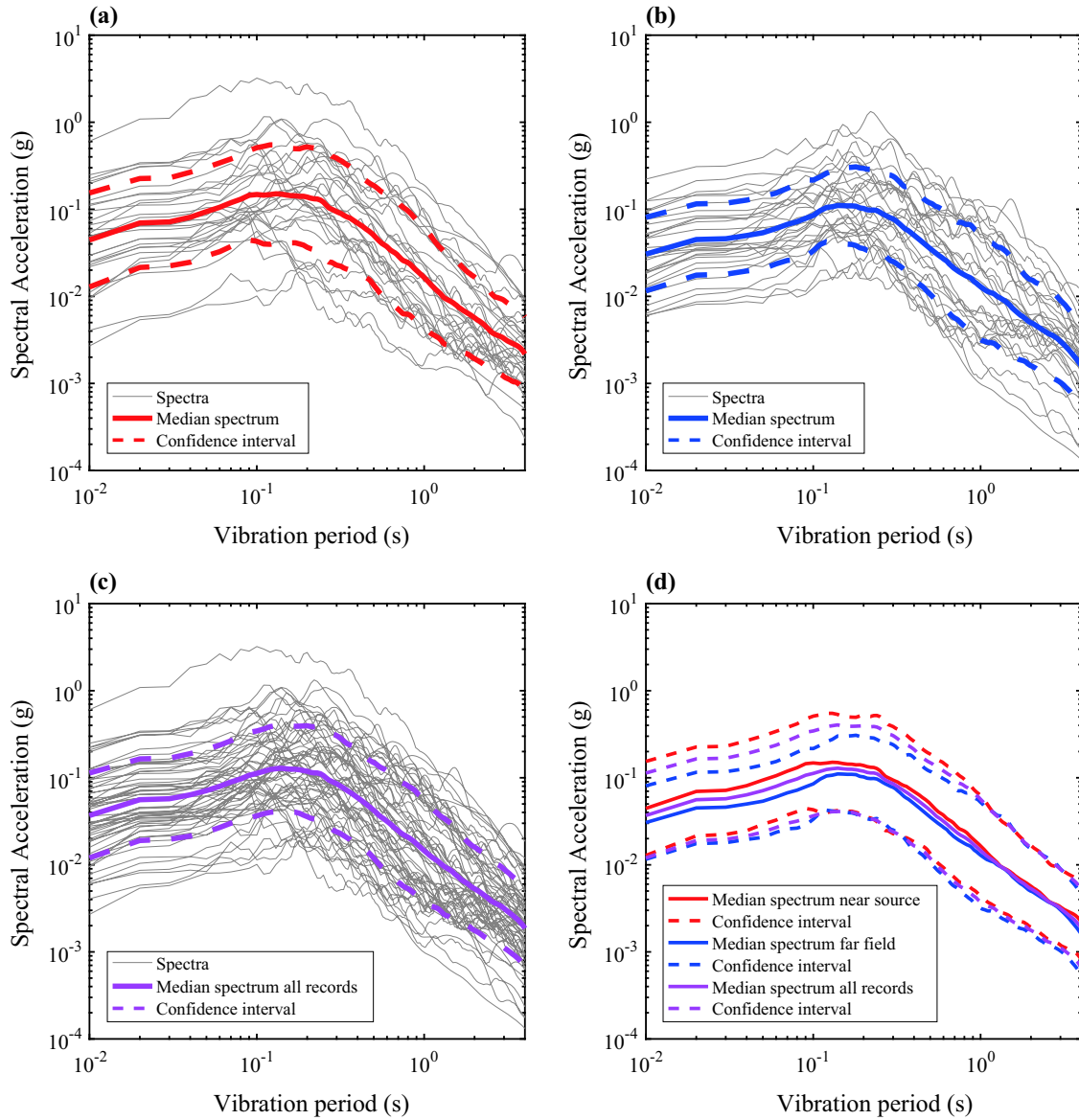
Fig. 10. Acceleration response spectra for the set (a) A, (b) B, and (c) both sets together; (d) overlay of the median spectra and of the associated confidence intervals of set A and B, and all records.
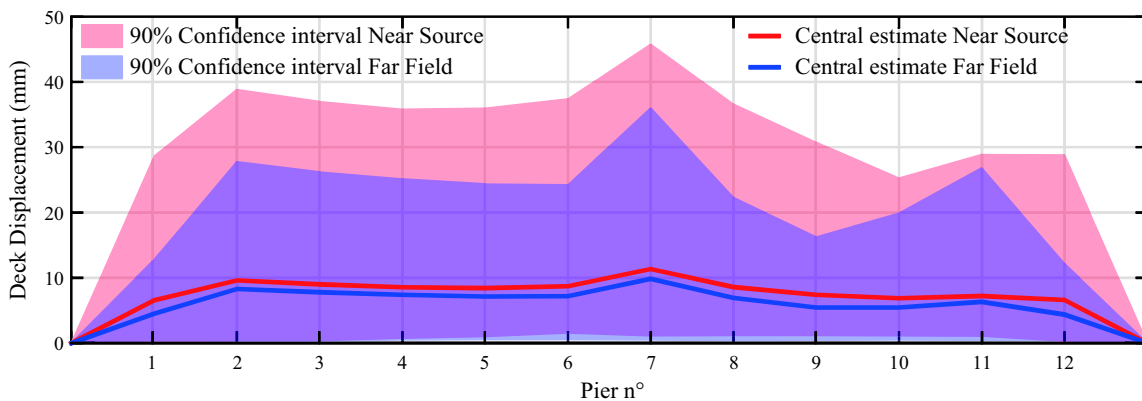
Fig. 11. Central estimates (mean) and confidence intervals of the deck displacements respectively for the set A (in red) and B (in blue). (For interpretation of the references to colour in this figure legend, the reader is referred to the web version of this article.)
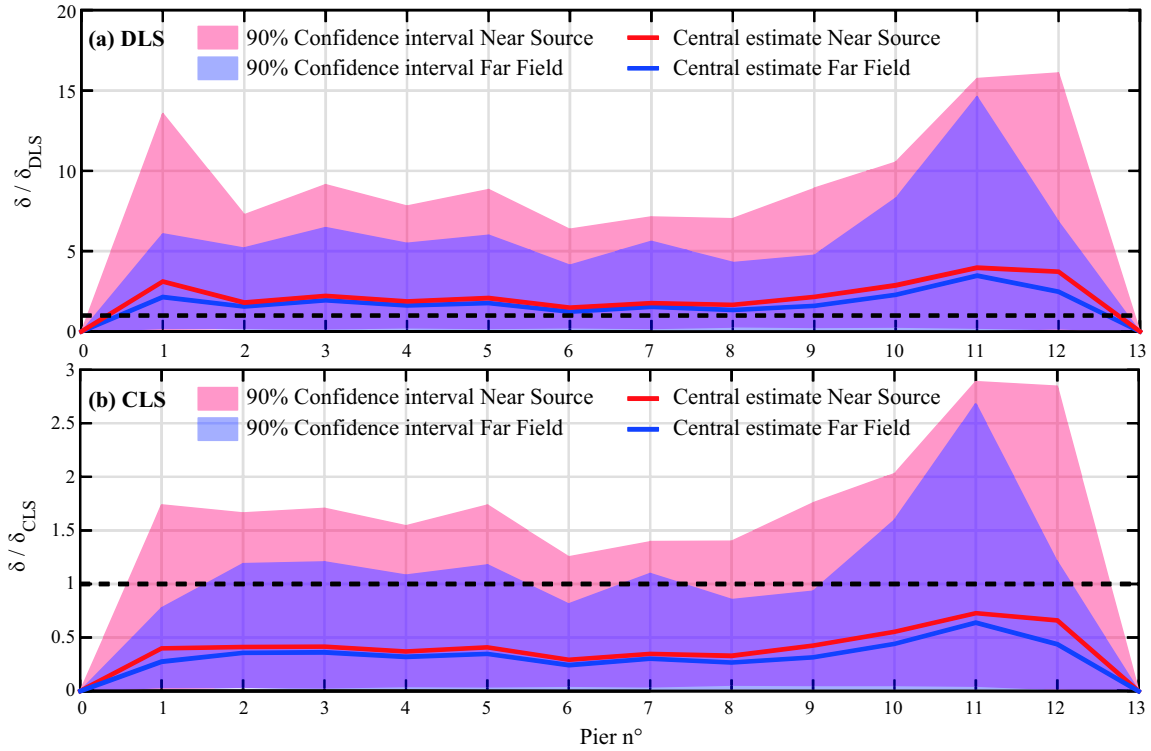
Fig. 12. Normalized mean transversal displacements (and 90% confidence interval) for the for near-source (red) and far-field (blue) records, and for damage limit state (top) and collapse limit state (bottom). (For interpretation of the references to colour in this figure legend, the reader is referred to the web version of this article.)
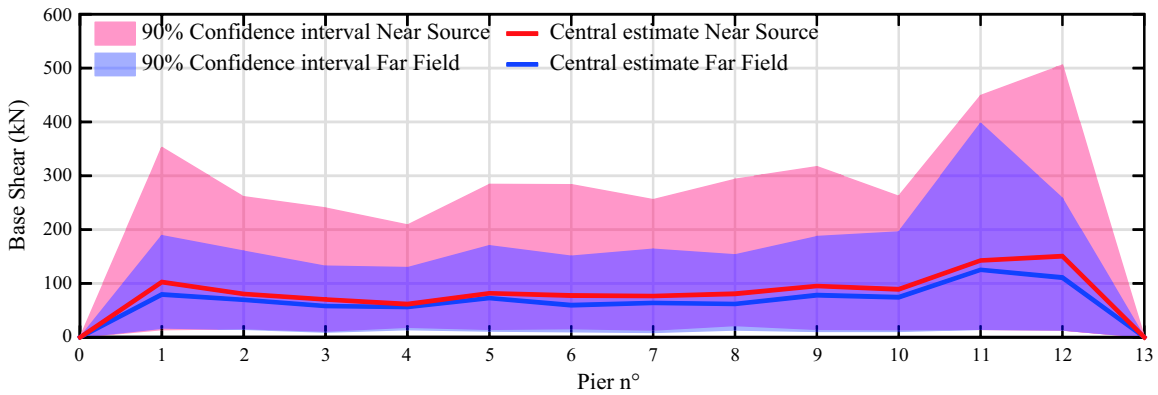
Fig. 13. Central estimates (mean) and confidence intervals of the base shear respectively for the set A (in red) and B (in blue).

Near-source and far-field records lead to the collapse 7 and 5 times, respectively. Such finding confirms the outcomes presented in Figs. 11–15. PGA values of far-field records are lower than PGA values of near source records, as observed in Tables 2 and 3, therefore, the linear regression associated to the second set of records (Set B) is lowered with respect to the first set of ground motions (Set A). Consequently the limit state (Y = 1) for the set B if reached for lower values of PGA with respect to the set A. The third set of records, as expected, presents results in between sets A and B. Fig. 17 illustrates the robust fragility curves and their confidence intervals obtained with Cloud analysis for the two limit states above presented, considering both the flexural and overall demand-over-capacity ratios. Moreover, Table 4 shows the statistics (i.e. η and β, respectively the median and the logarithmic standard deviation) of the 50th percentile fragility curves.

It is worth noting that the fragility response tends to be more conservative when the brittle failure is considered, with a reduction of the median capacity of about 25 times for the damage limitation and a reduction between 10 and 17 times for the collapse limit state. Moreover, moving from the pure flexural to the overall critical demand-over-capacity ratio there is a reduction of the confidence interval. In accordance with the linear regression, the dispersion of the fragility curves obtained for the set A is smaller than the dispersion of the curves obtained for the set B. Set A presents a larger value of the median of the 50th percentile fragility with respect to set B (this result is in line with the characteristics of the linear regressions discussed before); thus the bridge tends to be slightly more sensitive to the Set B.

The greater sensibility to the far-field set of records may be attributed to the earthquakes contained in Set B which possess, on average, a greater magnitude and greater dominant and mean periods with respect to Set A. As a result, the energy contained in the strong motions of Set B is on average larger, and the frequency characteristics of the signals are closer to the frequency character-
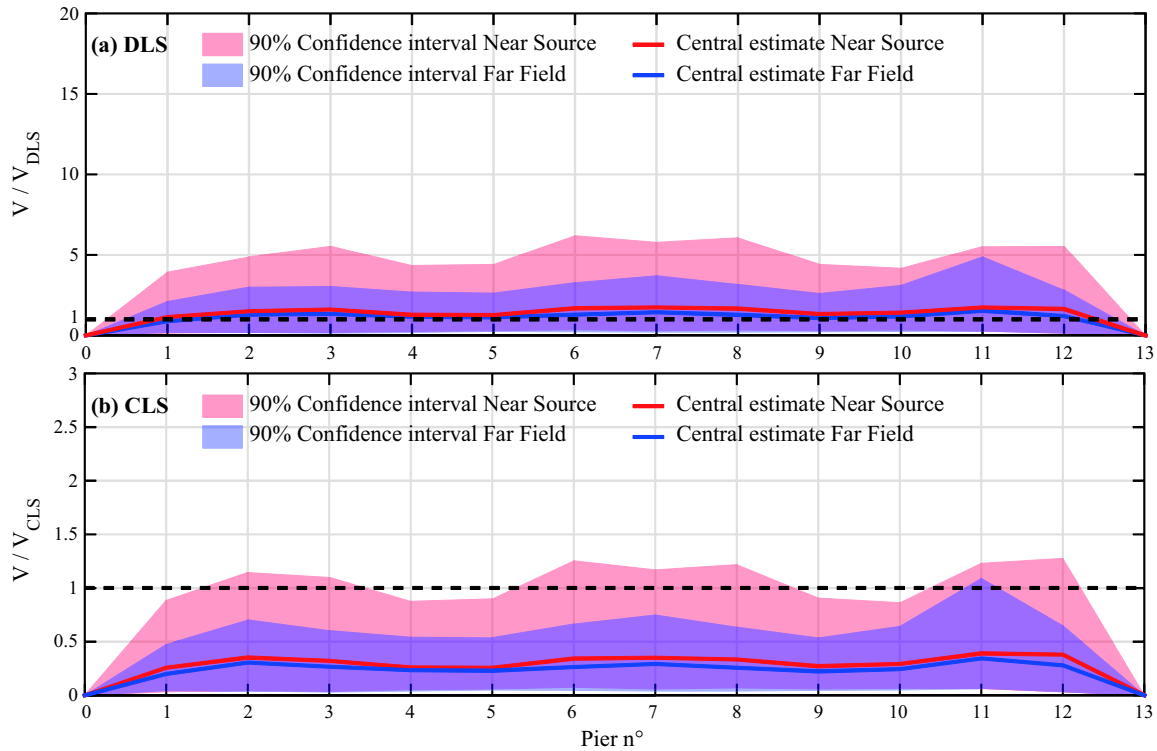
Fig. 14. Normalized mean base shear (and 90% confidence interval) for the for near-source (red) and far-field (blue) records, and for damage limit state (top) and collapse limit state (bottom). (For interpretation of the references to colour in this figure legend, the reader is referred to the web version of this article.)
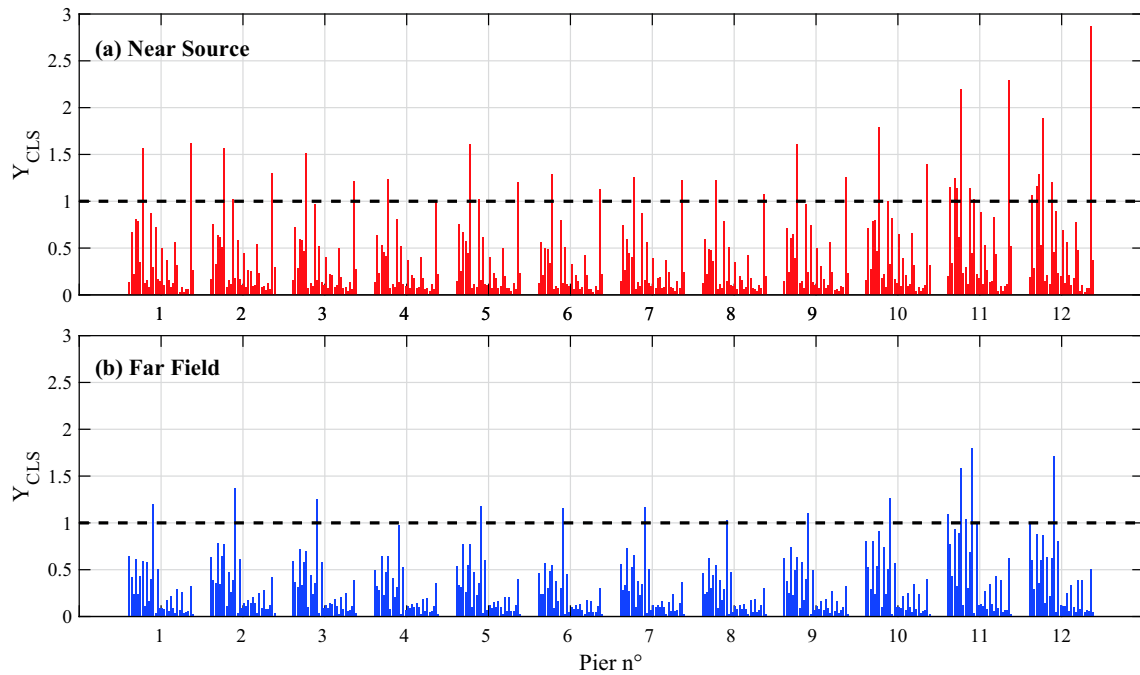
Fig. 15. Maximum demand-over-capacity ratio for each pier, for each accelerogram and for both the set of accelerograms.

istics of the structural system. This observation confirms that more deformable systems are more sensitive to far field events rather than near source events. Therefore, even if the Set B presents ground motions with lower values of PGA (lowering the linear regression) the probability of observing the failure is higher with respect to the Set A, for the same value of PGA. On the other hand,

the lowering effect due to the smaller value of PGA in the linear regression can be criticized as the responsible of such a result. Conversely, if the infrastructure manager or the decision maker of the traffic network can distinguish between far-field and near-source earthquake in the aftermath of an event, and the value of the intensity measure is known at the site of the bridge, he/she can make
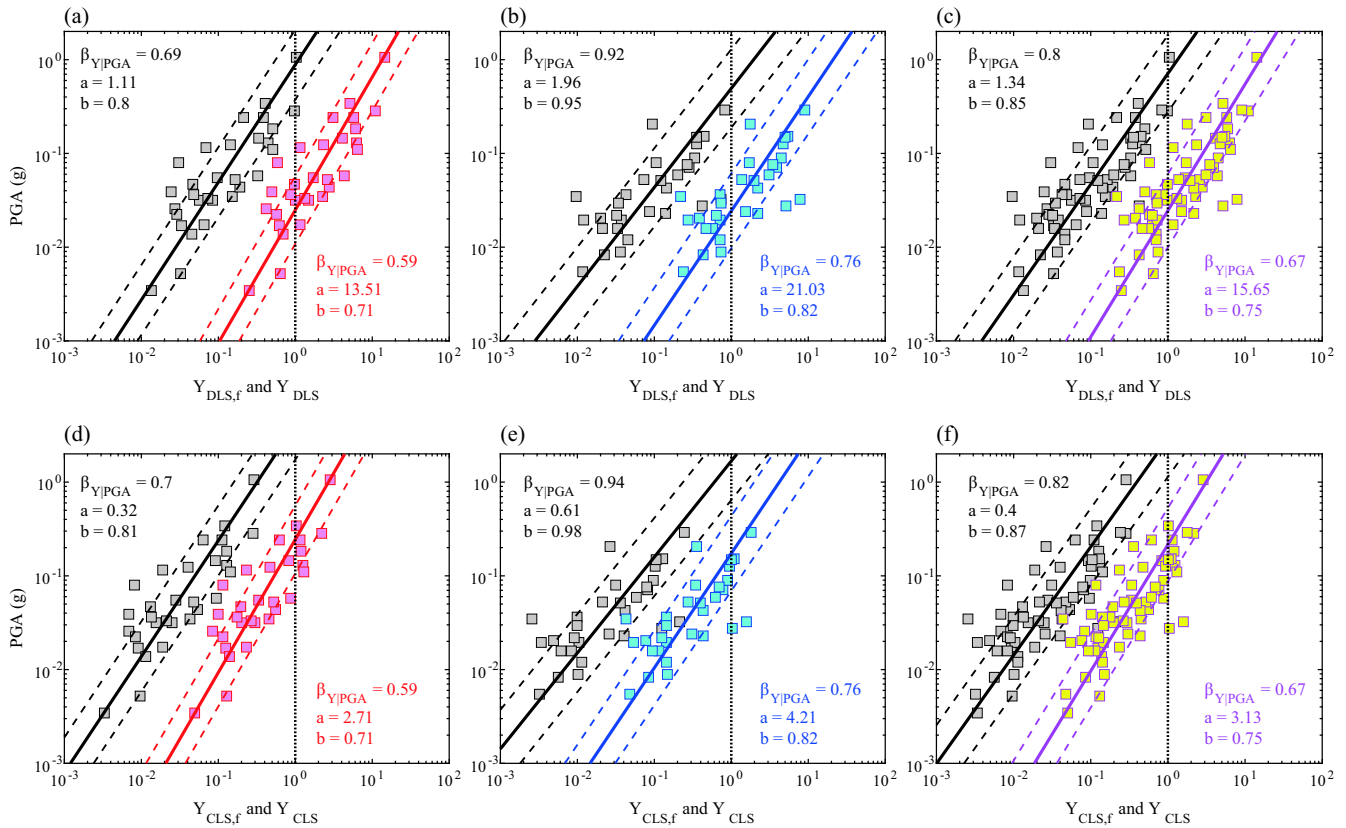
Fig. 16. Cloud Analysis for maximum ductile (black lines) and brittle (coloured lines) Y versus peak ground acceleration, for the DLS (a–c) and CLS (d–f), for near-source (a, d), far-field (b, e), and (c, f) all ground motions.

more robust probabilistic analysis having two fragilities corresponding to the two different sets. For sake of completeness, also the fragility curves corresponding to the set of strong motions containing both set A and B is presented. Such fragility can be used independently from the typology of the event.

6.2. IDA-based fragility curves

The Cloud analysis has emphasized the importance of including the brittle failure in the seismic assessment of the sample bridge system thus for the IDA results only the overall Y is taken into account. Fig. 18 represents the IDA curves (the gray lines) obtained for the two limit states and for the three sets of ground motions used herein. On the same plot three curves representative of the statistics, i.e. the median (the thicker colored continuous lines), the 16th and the 84th percentiles (the thicker dashed colored lines), are also shown.

The square markers represent the intersection of the IDA curves with Y = 1, and their distributions are presented as probability density function on the vertical axis. Finally, the cloud data are overlaid on the previous curves as black dots. It is worth noting that such black dots are located exactly on the IDA curves, thus indicating the reliability of the analyses.

The robust fragility curve was built according to Jalayer et al. [36]. Fig. 19 provides the robust fragility curves and their confidence intervals obtained with IDA for the DLS and CLS, considering only the overall critical demand over-capacity-ratio.

Statistics of the central fragility curves are listed in Table 5. Higher values of the median of the central fragility are obtained for Set A records with respect to Set B. Such outcome is compliant with the results of the Cloud analysis discussed earlier, but the differences are smaller, and the two fragilities corresponding to Set A

and Set B are close to the fragility obtained considering all the record together. Moreover, also in this case the fragility dispersion is higher for Set B than for Set A.

6.3. Comparison between Cloud and IDA

For the ductile and brittle failure modes, fragility curves are governed by the failure of the elements at the first level (column and beams) of the piers close to the abutments, i.e. the piers #1, 2, 11 and 12, as illustrated in Section 5. These findings apply to both Cloud and IDA analyses. It is worth comparing the fragility curves (representative of the same ground motion set and the same limit state) obtained with the Cloud and IDA procedures, respectively. Fig. 20 illustrates the median fragility curves for the two procedures applied for the two limit states and for the three sets utilized.

The matching between the two curves for the different cases is satisfactory for the damage limit state (Fig. 20a–c) and for the collapse limit state for set B (Fig. 20e); notwithstanding, some mismatches can be observed for collapse limit state for set A (Fig. 20d) and consequently for the set containing all the records (Fig. 20f). The less conservative fragility curves (i.e. larger values of capacity for the same probability value) obtained with the Cloud analysis for the CLS, is due to the properties of the selected records. Conversely, the IDA analysis, is able to identify the onset of the non-linear behaviour. Additionally, such analysis can also detect the damageability limit state with higher accuracy [69,70]. The damage limit state is a limit state that is strictly correlated to the transitability (functionality) of the bridge [2].

As a result, in a framework of rapid structural assessment, given that the Cloud analysis is less time-consuming than the IDA (with a time ratio larger than one over the number of steps of scaling), it is
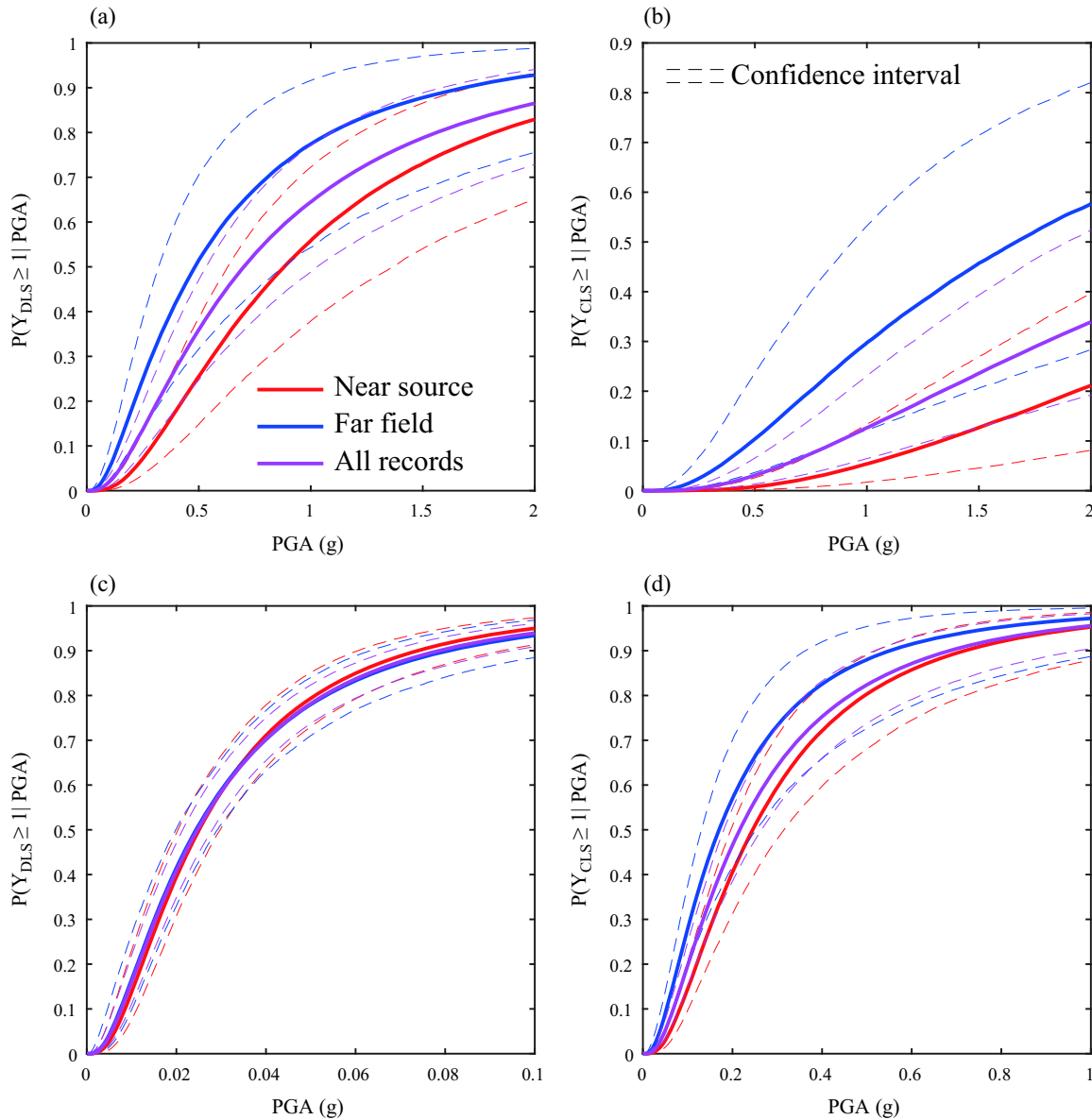
Fig. 17. The robust fragility curves based on Cloud analysis considering all sets of accelerograms, obtained considering only flexural mechanism (a, b) and both flexural and brittle failures (c, d).

Table 4
The 50th percentile fragility curve statistics for the two limit states and for the three sets considered.

Set	Mechanism	η_{PGA} (DLS) (g)	β_{PGA} (DLS) (−)	η_{PGA} (CLS) (g)	β_{PGA} (CLS) (−)
A	Flexural	0.88	0.86	4.12	0.54
	Flexural & Brittle	0.03	0.86	0.24	0.83
B	Flexural	0.49	0.97	1.69	0.97
	Flexural & Brittle	0.02	0.93	0.17	0.91
A & B	Flexural	0.70	0.94	2.97	0.95
	Flexural & Brittle	0.03	0.90	0.22	0.90

essential to select an appropriate set of accelerograms to estimate reliably the damage occurrence and pattern.

6.4. Pier-by-pier fragility curves: the systemic evaluation of the bridge vulnerability

The IDA results are used herein to compare the whole bridge fragility curve, representative of the bridge as a system, with the pier-by-pier fragilities, obtained considering separately the response of each pier; Fig. 21 shows such comparisons with respect the CLS.

It is worth noting that since the adopted engineering demand parameter Y is based on the reliability theory of the cut-sets, i.e. a series of parallel system, the fragility curve for the whole bridge (the thicker curve in Figs. 21a and b) is close, but not coincident, to the more critical piers, that in this case are the piers #9, 11, and 12.
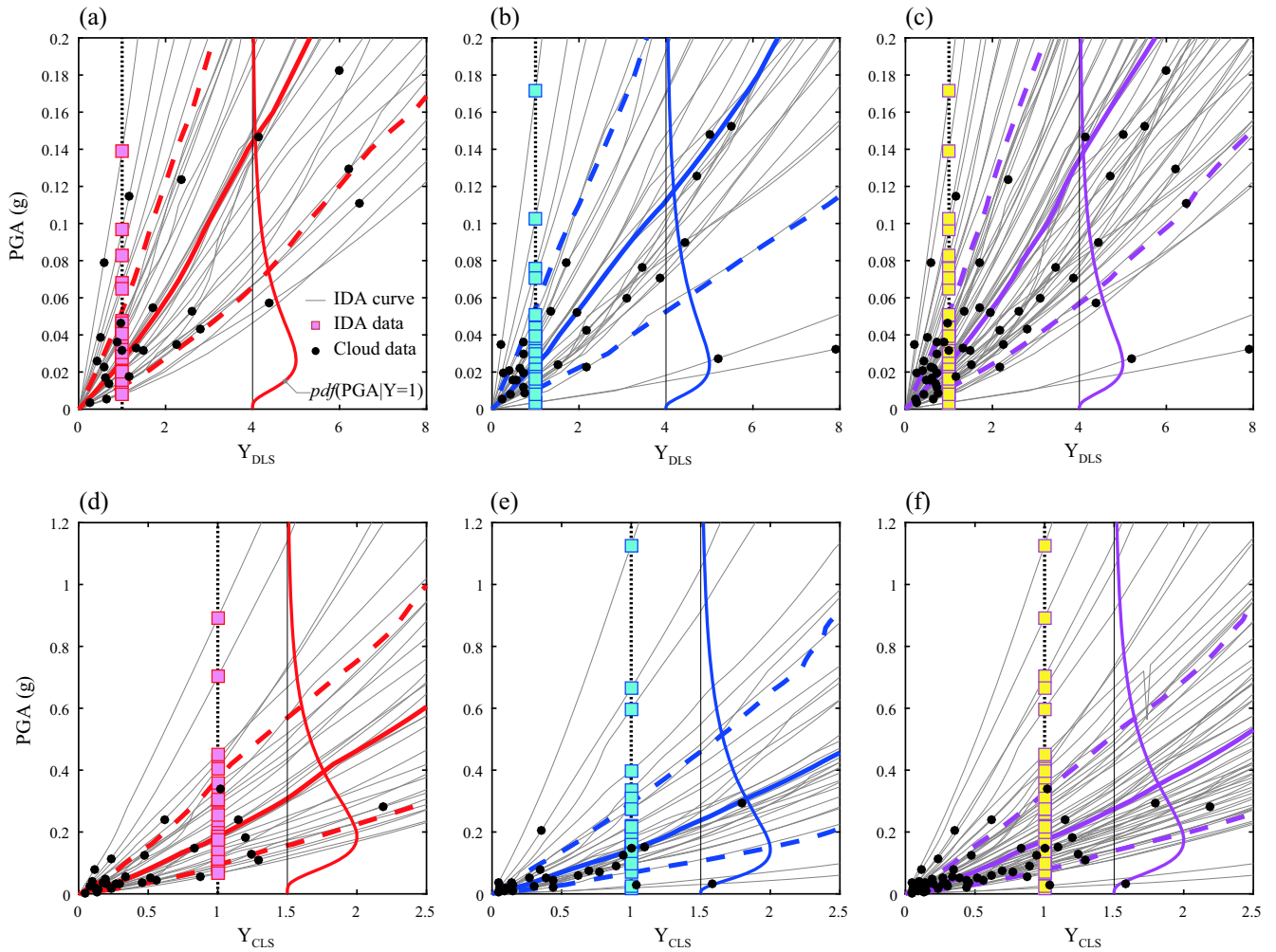
Fig. 18. IDA curves for DLS (a, c) and CLS (b, d), and for both sets of accelerograms, i.e. Near source (a, b) and Far field (c, d). The coloured ticker lines represents the curves statistics, i.e. median, 16th, and 84th percentile curves.
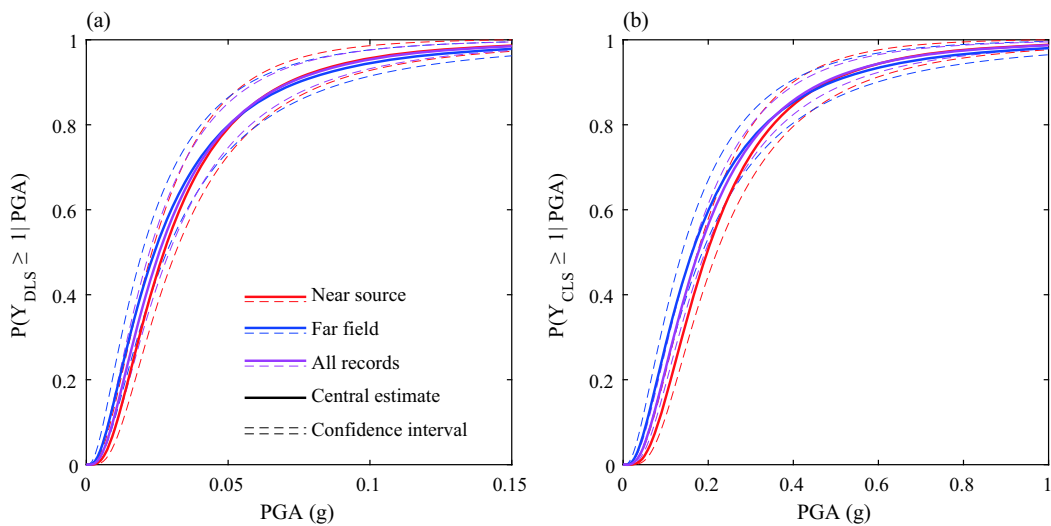
Fig. 19. The robust fragility curves based on IDA considering both sets of accelerograms for DLS (a) and CLS (b).

Such representation is very useful for structural retrofitting purposes. It is evident that if local mitigation strategies, such as shear strengthening with fiber reinforced material for shear critical elements of the piers, are applied to the critical piers, an increase of the mean capacity of 50% for the whole bridge can be obtained. For more onerous and/or advanced retrofitting strategies, such as columns jacketing, or additional dissipation, new analyses of the entire system need to be performed.

Table 5
The 50th percentile fragility curve statistics for the two limit states and for the two sets considered, related to YLS.

Set	η_{PGA} (DLS) (g)	β_{PGA} (DLS) (−)	η_{PGA} (CLS) (g)	β_{PGA} (CLS) (−)
A	0.03	0.71	0.20	0.68
B	0.02	0.83	0.17	0.85
A & B	0.03	0.79	0.18	0.7
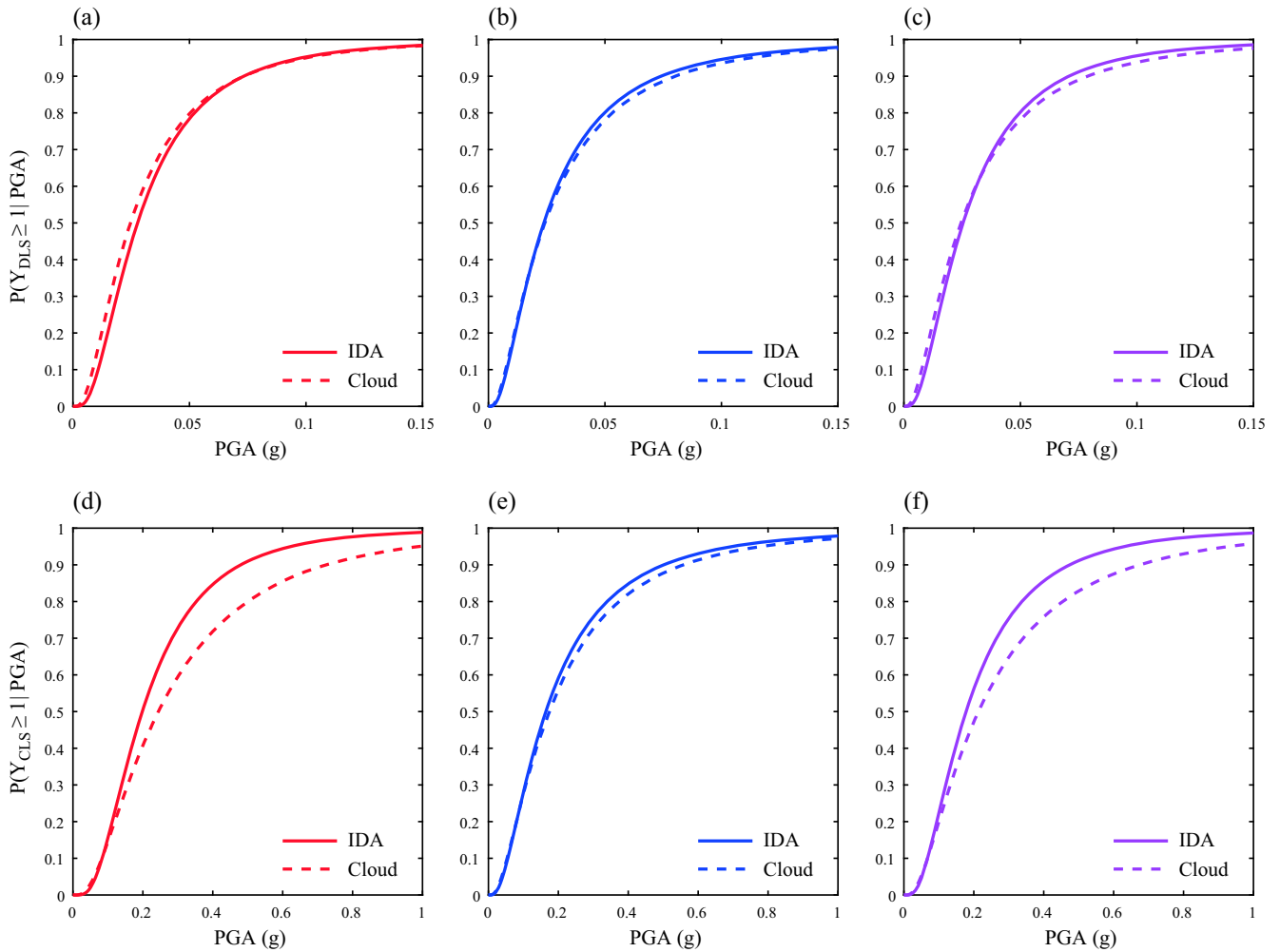
Fig. 20. The robust fragility curves based on IDA (continuous lines) and Cloud (dashed lines) considering both sets of accelerograms, and for all the records together, for DLS (a–c) and CLS (d–f).
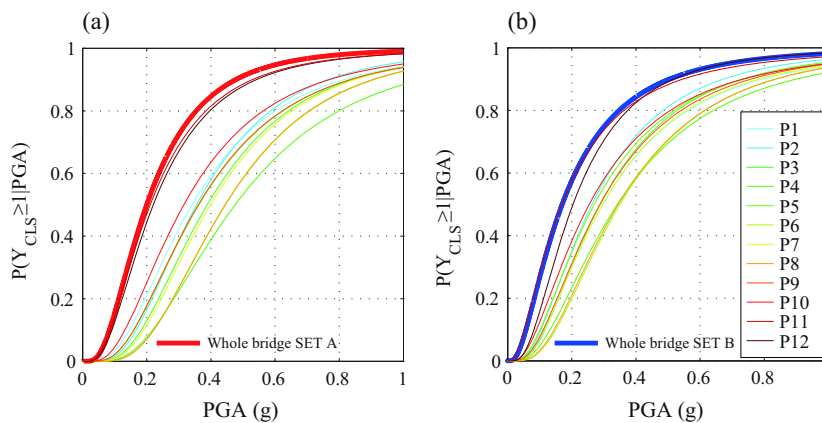
Fig. 21. Pier-by-pier collapse fragility compared with the whole bridge fragility for near-source (a) and far-field (b) ground motions.
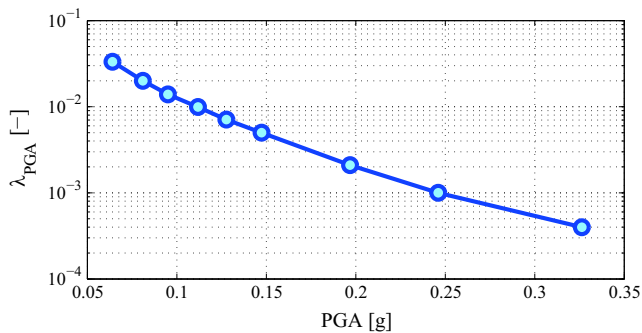
Fig. 22. The hazard curve.

Table 6
Return period associated to the predefined limit states.

	$T_{R,DLS}$ (Ys)	$T_{R,CLS}$ (Ys)
Set A	19	152
Set B	16	90
Sets A & B	18	110

6.5. Risk indicator

The structural performance could be quantified also in terms of mean annual rate of exceedance of the predefined limit states (λ_{LS}) or, alternatively, in terms of return period ($T_{R,LS} = 1/\lambda_{LS}$), that can be considered as vulnerability indicator. Integrating the IDA-based fragility curves with the seismic hazard curve (shown in Fig. 22) for the bridge location (obtained in compliance with the National Annex to Italian building codes [19], the results presented in Table 6 have been obtained.

As stated earlier, it is found that Set A is less conservative that Set B, and the values of return periods are well below the values of return period generally expected for the considered damage states, i.e. 50 years for the DLS and 475 years for the CLS.

7. Conclusions

The seismic assessment of an existing Italian RC bridge with portal-frame piers, designed for gravity loads only has been presented. A simple yet efficient methodology for the sample bridge is proposed as well. Such procedure is versatile and sound for the implementation in codes of practice. Two structural limit states were defined: the damage limit state (DLS) and the collapse limit state (CLS). The analysis scheme encompasses reliable capacity formulations for the transversal section of the structural elements. Therefore, adequate formulations for the evaluation of the structural capacity of the structural elements of the portal frames of the piers have been considered. A new definition for brittle DLS capacities is proposed, based on the CLS formulation.

The seismic response of the sample bridge structure has been investigated through dynamic non-linear analyses. Moreover, fragilities have been derived through comprehensive and efficient procedures, such as Cloud and IDA. Two sets of 30 strong motion records have been used to study the effects of far-field and near-source strong motions. Moreover, for sake of completeness, an additional set of 60 strong motions obtained combining the two previous sets, has been adopted.

It was observed that the brittle failure of the transverse beams of piers governs the bridge response. Additionally, the comprehensive numerical investigations carried out in the present work show that, on average, the near-source strong motions tend to impose

higher and more variable inelastic demand on fragile components of the bridge system than far-field records. Nevertheless, the fragility curves relative to the latter records exhibit higher probability of failure than the near-source strong motion counterparts. Such results comply with recent observations presented in the literature.

For the damage assessment, it is found that the Cloud analysis lead to fragility curves similar to those derived through the IDA procedure. Conversely, different response can be estimated with the Cloud and IDA procedures for the collapse limit state for near-source records. In a framework of rapid structural assessment, given that the Cloud analysis is less time-consuming than the IDA, it is essential to select an appropriate set of accelerograms to estimate reliably the damage occurrence and pattern, considering also that the damage limit state is strictly correlated to the functionality of the bridge. With respect to the Cloud analyses, the records selected for the analyzed case study are suitable for the damage limit state. However, they have lower reliability when assessing the collapse limit state, for which different records are potentially required.

Finally, a new pier-by-pier fragility methodology, representing the breakdown of the whole bridge fragility, has also been discussed. Such tool is efficient to prioritize structural interventions on the bridge piers. It is envisaged that the correlation between the structural responses of the single piers should also be considered in order to describe the whole bridge in a more refined manner.

The structural performance has been also computed in terms of mean annual rate of exceedance of the prescribed limit states. It emerged that, according to the assumed hypotheses, the bridge can be considered under-standard.

References

[1] Abbiati G, Bursi OS, Caperan P, Di Sarno L, Molina FJ, Paolacci F, et al. Hybrid simulations of a multi-span RC viaduct with plain bars and sliding bearings. Earthquake Eng Struct Dynam 2015;44(13):2221–40.
[2] Alessandri S, Giannini R, Paolacci F. Aftershock risk assessment and the decision to open traffic on bridges. Earthquake Eng Struct Dynam 2013;42 (15):2255–75.
[3] Ambraseys NN, Smit P, Douglas J, Margaris B, Sigbjörnsson R, Olafsson S, et al. Internet site for European strong-motion data. Boll Geofis Teorica Appl 2004;45(3):113–29.
[4] Basoz NI, Kiremidjian AS, King SA, Law KH. Statistical analysis of bridge damage data from the 1994 Northridge, CA, earthquake. Earthq Spectra 1999;15:25–54.
[5] Benjamin JR, Cornell CA. Probability, statistics and decision for civil engineers. New York: McGraw-Hill; 1975.
[6] Bentz E, Collins MP. Response-2000 user manual. Toronto, Canada: University of Toronto; 2001.
[7] Biskinis D, Fardis MN. Stiffness and cyclic deformation capacity of circular RC columns with or without lap-splices and FRP wrapping. Bull Earthq Eng 2013;11(5):1447–66.
[8] Borzi B, Ceresa P, Franchin P, Noto F, Calvi GM, Pinto PE. Seismic vulnerability of the Italian roadway bridge stock. Earthq Spectra 2015;31(4):2137–61.
[9] Broderick BM, Elnashai AS, Ambraseys NN, Barr JM, Goodfellow RG, Higazy EM. The Northridge (California) Earthquake of 17 January 1994: Observations, Strong Motion and Correlative Response Analysis. Engineering Seismology and Earthquake Engineering, Research Report No. ESEE 94/4, Imperial College, London; 1994.

[10] Cardone D, Perrone G, Sofia S. A performance-based adaptive methodology for the seismic evaluation of multi-span simply supported deck bridges. Bull Earthq Eng 2011;9(5):1463–98.

[11] CEN. Comité Européen de Normalisation, Eurocode 8: Design of structures for earthquake resistance—Part 1: General rules, seismic actions and rules for buildings. EN 1:2004; 2004.

[12] CEN. Comité Européen de Normalisation, Eurocode 8: Design of structures for earthquake resistance—Part 3: Assessment and retrofitting of buildings, Bruxell; 2006.

[13] Chang KC, Chang DW, Tsai MH, Sung YC. Seismic performance of highway bridges. Earthq Eng Eng Seismol 2000;2(1):55–77.

[14] Choi E, DesRoches R, Nielson B. Seismic fragility of typical bridges in moderate seismic zones. Eng Struct 2004;26(2):187–99.

[15] Cimellaro GP, Reinhorn AM, D'Ambrisi A, De Stefano M. Fragility analysis and seismic record selection. J Struct Eng 2009;137(3):379–90.

[16] Cornell CA, Krawinkler H. Progress and challenges in seismic performance assessment. PEER Center News 2000;3(2):1–4.

[17] Cornell CA, Jalayer F, Hamburger RO, Foutch DA. Probabilistic basis for 2000 SAC federal emergency management agency steel moment frame guidelines. J Struct Eng 2002;128(4):526–33.

[18] Cosenza E, Manfredi G. Damage indices and damage measures. Prog Struct Mat Eng 2000;2(1):50–9.

[19] DD.LL. Decreto Ministeriale del 14 gennaio 2008. Approvazione delle nuove norme tecniche per le costruzioni. G.U. n. 29 del 4/2/2008 [in Italian]; 2008.

[20] De Bortoli M, Zareian F, Shantz T. Significance of ground motion incidence angle in seismic design of bridges, NCEE 2014–10th U.S. National Conference on Earthquake Engineering: Frontiers of Earthquake Engineering, NCEE 2014; Anchorage; United States; 21 July 2014 through 25 July 2014; 2014.

[21] Della Corte G, De Risi R, Di Sarno L. Approximate Method for Transverse Response Analysis of Partially Isolated Bridges. J Bridge Eng 2013;18 (11):1121–30.

[22] Del Vecchio C, Kwon OS, Di Sarno L, Prota A. Accuracy of nonlinear static procedures for the seismic assessment of shear critical structures. Earthquake Eng Struct Dynam 2015;44(10):1581–600.

[23] Di Sarno L, Del Vecchio C, Maddaloni G, Prota A. Shake table studies of an as-built RC bridge with smooth bars. Eng Struct 2017;136:355–68.

[24] Ditlevsen O, Masden H. Structural Reliability Methods. New York: Wiley; 1996.

[25] Elefante L, Jalayer F, Iervolino I, Manfredi G. Disaggregation-based response weighting scheme for seismic risk assessment of structures. Soil Dyn Earthq Eng 2010;30(12):1513–27.

[26] Elnashai AS, Bommer JJ, Baron I, Salama AI, Lee D. Selected Engineering Seismology and Structural Engineering Studies of the Hyogo-ken Nanbu (Kobe, Japan) Earthquake of 17 January 1995. Engineering Seismology and Earthquake Engineering, Report No. ESEE/95-2, Imperial College, London; 1995.

[27] Enright MP, Frangopol DM. Survey and evaluation of damaged concrete bridges. J Bridge Eng 2000;5(1):31–8.

[28] Fardis MN. Seismic design, assessment and retrofitting of concrete buildings: based on EN-Eurocode 8, vol. 8. Springer; 2009.

[29] FIB, Federation Internationale du Beton. Seismic bridge design and retrofit-structural solutions. FIB Bull 39; 2007.

[30] FHWA, Federal Highway Administration. Seismic retrofitting manual for highway structures: Part I – Bridges. Publication No.FHWA-HRT-06-032, Research, Development and Technology Tuner-Fairbank Highway Research Center, McLean, VA; 2006.

[31] Franchetti P, Grendene M, Sleiko D, Modena C. Seismic damage assessment for six RC bridges in the Veneto region (NE Italy). Boll Geofis Appl 2008;49(3–4):513–32.

[32] Franchin P, Lupoi A, Noto F, Tesfamariam S. Seismic fragility of reinforced concrete girder bridges using Bayesian belief network. Earthquake Eng Struct Dynam 2016;45(1):29–44.

[33] Haskett M, Oehlers DJ, Ali MM, Sharma SK. Evaluating the shear-friction resistance across sliding planes in concrete. Eng Struct 2011;33(4):1357–64.

[34] Hwang H, Liu J-B, Chiu Y-H. Seismic fragility analysis of highway bridges. Report. Center for Earthquake Research and Information; 2001.

[35] Iervolino I, De Luca F, Chioccarelli E. Engineering seismic demand in the 2012 Emilia sequence: preliminary analysis and model compatibility assessment. Ann Geophys 2012;55(4):639–45.

[36] Jalayer F, De Risi R, Manfredi G. Bayesian Cloud Analysis: Efficient structural fragility assessment using linear regression. Bull Earthq Eng 2015;13 (4):1183–203.

[37] Jalayer F, Elefante L, Iervolino I, Manfredi G. Knowledge-based performance assessment of existing RC buildings. J Earthquake Eng 2011;15(3):362–89.

[38] Kappos AJ, Saiidi MS, Aydınoğlu MN, Isaković T. (Eds.). Seismic Design and Assessment of Bridges – Inelastic Methods of Analysis and Case Studies. Series: Geotechnical, Geological and Earthquake Engineering, vol. 21, Springer; 2012.

[39] Kaviani P, Zareian F, Taciroglu E. Seismic behavior of reinforced concrete bridges with skew-angled seat-type abutments. Eng Struct 2012;45:137–50.

[40] Kawashima K, Unjoh S, Hoshikuma J, Kosa K. Damage of bridges due to the 2010 Maule, Chile Earthquake. J Earthquake Eng 2010;15(7):1036–68.

[41] Li J, Peng T, Xu Y. Damage investigation of girder bridges under the Wenchuan earthquake and corresponding seismic design recommendations. Earthq Eng Eng Vibr 2008;7(4):337–44.

[42] Lu DG, Yu X-H, Pan F, Wang G-Y. Probabilistic seismic demand analysis considering random system properties by an improved cloud method. In: Proceedings of the 14th World Conference on Earthquake Engineering, Beijing, China (CD-ROM); 2008.

[43] Lupoi A, Franchin P, Schotanus M. Seismic risk evaluation of RC bridge structures. Earthquake Eng Struct Dynam 2003;32(8):1275–90.

[44] Mackie J, Stojadinovic B. Probabilistic seismic demand for California highway bridges. J Bridge Eng 2001;6(6):468–81.

[45] Mander JB, Priestley MJ, Park R. Theoretical stress-strain model for confined concrete. J Struct Eng 1988;114(8):1804–26.

[46] Miano A, Jalayer F, De Risi R, Prota A, Manfredi G. Model updating and seismic loss assessment for a portfolio of bridges. Bull Earthq Eng 2016;14 (3):699–719.

[47] McKenna F. OpenSees: a framework for earthquake engineering simulation. Comput Sci Eng 2011;13(4):58–66.

[48] Mobasher B, Omrani R, Taciroglu E, Zareian F. Validated macroelement models for abutment shear keys and seismic response sensitivity of ordinary bridges to shear key behavior. Eng Struct 2016.

[49] Moehle J, Fenves G, Mayes R, Priestley N, Seible F, Uang CM, et al. Highway bridges and traffic management. Earthq Spectra 1995;11(S2):287–372.

[50] Moehle J, Deierlein GG. A framework methodology for performance-based earthquake engineering. In: Proceedings of the 13th World Conference on Earthquake Engineering. Vancouver, Canada (CD-ROM); 2004.

[51] Mosleh A, Razzaghi MS, Jara J, Varum H. Seismic fragility analysis of typical pre-1990 bridges due to near-and far-field ground motions. Int J Adv Struct Eng 2016;8(1):1–9.

[52] Nielson BG, DesRoches R. Analytical seismic fragility curves for typical bridges in the central and southeastern United States. Earthq Spectra 2007;23 (3):615–33.

[53] Nielson BG, DesRoches R. Seismic fragility methodology for highway bridges using a component level approach. Earthquake Eng Struct Dynam 2007;36 (6):823–39.

[54] Padgett JE, Nielson BG, DesRoches R. Selection of optimal intensity measures in probabilistic seismic demand models of highway bridge portfolios. Earthquake Eng Struct Dynam 2008;37(5):711–25.

[55] Paolacci F, Giannini R. An experimental and numerical investigation on the cyclic response of a portal frame pier belonging to an old reinforced concrete viaduct. Earthquake Eng Struct Dynam 2012;41(6):1109–27.

[56] Paolacci F, Pegon P, Javier Molina F, Poljansek M, Giannini R, Di Sarno L, et al. Assessment of the seismic vulnerability of an old RC viaduct with frame piers and study of the effectiveness of base isolation through PsD testing (RETRO); 2014a. http://dx.doi.org/10.2788/63472.

[57] Paolacci F, Di Sarno L, Pegon P, Molina FJ, Poljansek M, Bursi OS, et al. Assessment of the seismic behaviour of a retrofitted old R.C. highway bridge through PsD testing. SERIES Concluding Workshop – Joint with US-NEES "Earthquake Engineering Research Infrastructures", JRC-Ispra, May 28–30, 2013; 2014b.

[58] Paolacci F, Di Sarno L, De Risi R, Abbiati G, Mohamad A, Malena M, et al. Refined and simplified numerical models of an isolated old highway bridge for PsD testing. SERIES Concluding Workshop – Joint with US-NEES "Earthquake Engineering Research Infrastructures", JRC-Ispra, May 28–30, 2013; 2014c.

[59] Priestley MJN, Seible F, Calvi GM. Seismic assessment of existing bridges. Wiley Online Library; 1994.

[60] Priestley MJN, Kowalsky MJ, Vu N, Mc Daniel C. Comparison of recent shear strength provisions for circular bridge columns. In: 5th Proceedings Caltrans Seismic Workshop; 1998.

[61] Ranzo G, Priestley MJN. Seismic performance of large RC circular hollow columns. In: Proc., 12th World Conf. on Earthquake Engineering; 2000.

[62] Rathje EM, Abrahamson NA, Bray JD. Simplified frequency content estimates of earthquake ground motions. J Geotech Geoenviron Eng 1998;124(2):150–9.

[63] Reluis. Linee guida e manuale applicativo per la valutazione della sicurezza sismica e il consolidamento dei ponti esistenti in c.a., Progetto DPC-Reluis 2005–2008 Linea 3: Valutazione e riduzione del rischio sismico di ponti esistenti [in italian]; 2009.

[64] Reza SM, Shahria Alam M, Tesfamariam S. Performance evaluation of a multi-span RC bridge with irregular column heights of varying ductility levels. Proc Ann Conf Can Soc Civ Eng 2012;2:1445–54.

[65] Scawthorn C. The Marmara Turkey Earthquake of August 17, 1999, Reconnaissance Report, MCEER Technical Report MCEER-00-0001, Buffalo, NY; 2000.

[66] Sextos AG, Pitilakis KD, Kappos AJ. Inelastic dynamic analysis of RC bridges accounting for spatial variability of ground motion, site effects and soil–structure interaction phenomena. Part 1: Methodology and analytical tools. Earthquake Eng Struct Dynam 2003;32(4):607–27.

[67] Sextos AG, Kappos AJ, Pitilakis KD. Inelastic dynamic analysis of RC bridges accounting for spatial variability of ground motion, site effects and soil–structure interaction phenomena. Part 2: Parametric study. Earthquake Eng Struct Dynam 2003;32(4):629–52.

[68] Shinozuka M, Feng MQ, Lee J, Naganuma T. Statistical analysis of fragility curves. J Eng Mech 2000;126(12):1224–31.

[69] Vamvatsikos D, Cornell CA. Incremental dynamic analysis. Earthquake Eng Struct Dynam 2002;31(3):491–514.

[70] Vamvatsikos D, Cornell CA. Applied incremental dynamic analysis. Earthq Spectra 2004;20(2):523–53.

[71] Verderame GM, Ricci P, Manfredi G, Cosenza E. Ultimate chord rotation of RC columns with smooth bars: some considerations about EC8 prescriptions. Bull Earthq Eng 2010;8(6):1351–73.

[72] Verdugo R. Comparing liquefaction phenomena observed during the 2010 Maule, Chile earthquake and 2011 Great East Japan. In: Proceedings of the international symposium on engineering lessons learned from the 2011 great east Japan earthquake, Tokyo, Japan, pp 707–718; 2012.

[73] Vintzēleou EN, Tassios TP. Mathematical models for dowel action under monotonic and cyclic conditions. Mag Concr Res 1986;38(134):13–22.

[74] Wotherspoon L, Bradshaw A, Green R, Wood C, Palermo A, Cubrinovski M, et al. Performance of Bridges during the 2010 Darfield and 2011 Christchurch Earthquakes. Seismol Res Lett 2011;82(6):950–64.

[75] Yashinsky M. Performance of bridge seismic retrofits during Northridge earthquake. J Bridge Eng 1998;3(1):1–14.

[76] Zelaschi C, Monteiro R, Marques M, Pinho Rr, Comparative analysis of intensity measures for reinforced concrete bridges, Second European Conference on Earthquake Engineering and Seismology (2ECEES), Istanbul, Turkey, August 25–29; 2014.

[77] Zhao J, Sritharan S. Modeling of strain penetration effects in fiber-based analysis of reinforced concrete structures. ACI Struct J 2007;104(2):133.